

Exploiting Potential Inversion for Photoinduced Multielectron Transfer and Accumulation of Redox Equivalents in a Molecular Heptad

Julia Nomrowski and Oliver S. Wenger*

Department of Chemistry, University of Basel, St. Johannis-Ring 19, 4056 Basel, Switzerland

Table of contents

Equipment and methods	S2
Synthesis and product characterization	S3
UV-Vis absorption spectroscopy of the heptad and some reference compounds	S15
Cyclic voltammetry of the heptad and some reference compounds	S16
Spectro-electrochemical studies	S19
Energy-level scheme	S21
Transient absorption spectroscopy in neat CH ₃ CN	S22
Determination of the quantum yield	S27
Transient absorption spectroscopy in presence of acid	S29
Driving-forces for proton transfer and PCET	S30
Photocatalysis studies of thiolate-disulfide interchange	S31
Isomers and shortest TAA-TAA distances	S38
References	S42

Equipment and methods

All commercially available reagents were used as received. Dry CH_2Cl_2 , THF and diethyl ether were obtained from a solvent purification system from Innovative Technology. All other dry solvents used for synthesis or spectroscopic measurements were purchased from Sigma Aldrich and used as received. Deuterated solvents for NMR spectroscopy were purchased from Cambridge Isotope Laboratories or Sigma Aldrich. Thin layer chromatography was performed on silica plates from Merck (60 F254). Column chromatography was performed on silica gel (40-63 μm , Silicycle).

^1H NMR spectra were recorded on a Bruker Advance III NMR spectrometer operating at 250 MHz, 400 MHz, 500 MHz or 600 MHz proton frequency, and ^{13}C spectra at 101 MHz on a Bruker Advance III spectrometer. All chemical shifts (δ) are given in ppm and referenced to residual solvent peaks.¹ Coupling constants are listed in Hz and the multiplicity is abbreviated as follows: singlet (s), doublet (d), doublet of doublets (dd), doublet of doublet of doublets (ddd), triplet (t), doublet of triplets (dt), triplet of doublets (td), quartet (q), and multiplet (m).

ESI mass spectra were recorded on a Bruker Esquire 3000plus ion-trap ESI-MS operating in positive mode. The high-resolution mass spectra were measured on a Bruker maXis 4G QTOF ESI spectrometer operating in positive mode by Dr. Heinz Nadig.

Elemental analyses were performed on a Vario Micro Cube instrument from Elementar by Ms. Sylvie Mittelheisser. Cyclic voltammetry measurements were performed with a Versastat3-200 potentiostat from Princeton Applied Research. Measurements were conducted in dry, Ar-purged CH_3CN or CH_2Cl_2 with tetra-*n*-butylammonium hexafluorophosphate (0.1 M) as supporting electrolyte. A three-electrode setup was used to measure cyclic voltammograms, containing a glassy carbon disc serving as working electrode, a silver wire as counter electrode and an SCE reference electrode. Spectro-electrochemical measurements were performed in a quartz cuvette with a platinum gauze working electrode, a platinum wire as counter electrode and an SCE reference electrode.

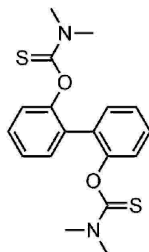
UV-Vis absorption spectra were measured on a Cary 5000 UV-Vis-NIR spectrophotometer. Transient absorption spectra were measured with an LP920-KS spectrometer from Edinburgh Instruments equipped with an iCCD camera from Andor. Single-wavelength kinetics were recorded using an R928 photomultiplier tube. A frequency-doubled Quantel Brilliant b laser served as excitation source. The duration of the laser excitation pulse was approximately 10 ns with a repetition frequency of 10 Hz. While the pulse energy used for transient absorption measurements on this setup is typically in the range of 12 to 15 mJ when using the standard laser output, for the measurements reported herein we employed a beam expander to irradiate a larger sample volume (essentially the entire cuvette) and increased to pulse energy to 40 to 50 mJ. Transient absorption spectra were time-averaged over a detection period of 100 ns directly after excitation unless otherwise stated. Quartz cuvettes from Starna were used for all optical measurements. To perform measurements under inert conditions, Schlenk cuvettes were used, and the solvent was degassed by four cycles of freeze-pump-thaw.

Photoredox catalysis experiments were performed in flame-sealed NMR tubes. Commercial DTT^{ox} was deuterated prior to use, by stirring it for 1 hour in D_2O , followed by removal of the solvent under reduced pressure, to minimize the amount of OH-signals in the NMR spectrum. The samples were prepared as follows: the substrate was dissolved in deuterated solvents, and the solutions were degassed by four cycles of freeze-pump-thaw. The solution was then filled into an NMR tube, frozen in a liquid nitrogen bath and the NMR tube sealed under vacuum using a hand-held gas burner. The samples were irradiated at 455 nm with an M455L2 LED from Thorlabs (3.5 W) at room temperature.

Synthesis and product formation

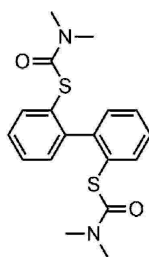
The syntheses and product characterization data of all compounds made in this work are reported in the following.

2,2'-Bis-*O*-(*N,N*-dimethylthiocarbamato)biphenyl ²



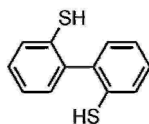
NaH (60% in oil, 520 mg, 13.0 mmol) was added in small portions to a solution of biphenyl-2,2'-diol (1.01 g, 5.42 mmol) in DMF (11 mL), and the mixture stirred at room temperature (rt) for 10 min under a nitrogen atmosphere. After addition of dimethylthiocarbamoyl chloride (2.10 g, 17.0 mmol), the solution was stirred for 3 h at 85 °C. After cooling to rt, aqueous NaHCO₃ solution was added. The white precipitate was filtered, washed with water, and dissolved in CH₂Cl₂. The organic solution was washed with water, dried over anhydrous Na₂SO₄, and the solvent removed under reduced pressure. Purification by column chromatography (SiO₂, pentane : EtOAc (7:3)), followed by recrystallization from acetone afforded the product as a white solid (684 mg, 35%). ¹H-NMR (400 MHz, CDCl₃): δ 7.45 - 7.34 (m, 4H), 7.26 (td, *J* = 7.5, 1.3 Hz, 2H), 7.23 - 7.15 (m, 2H), 3.26 (s, 6H), 3.03 (s, 6H) ppm.

2,2'-Bis-*S*-(*N,N*-dimethylthiocarbamato)biphenyl ³



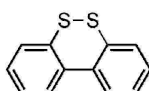
2,2'-Bis-*O*-(*N,N*-dimethylthiocarbamato)biphenyl (370 mg, 1.03 mmol) was dissolved in tetradecane (2 mL) and heated at 270 °C for 2.3 h under a nitrogen atmosphere. Purification by column chromatography (SiO₂, pentane : EtOAc (1:1)) afforded the product as a white solid (192 mg, 52%). ¹H-NMR (400 MHz, CDCl₃): δ 7.66 - 7.56 (m, 2H), 7.45 - 7.33 (m, 4H), 7.34 - 7.24 (m, 2H), 2.88 (s, 12H) ppm.

2,2'-Dimercaptobiphenyl⁴



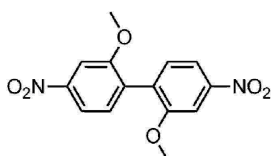
A solution of 2,2'-bis-S-(*N,N*-dimethylthiocarbamato)biphenyl (184 mg, 0.51 mmol) in dry THF (8 mL) was added to a mixture of LiAlH_4 (194 mg, 5.11 mmol) in dry THF (1.6 mL) at 0 °C. After complete addition, the mixture was heated at 65 °C for 6.5 h under a nitrogen atmosphere, followed by addition of aqueous HCl-solution (5-10 v%). The product was then extracted into Et_2O , the organic phase was dried over anhydrous Na_2SO_4 , and the solvent removed under reduced pressure. Purification by column chromatography (SiO_2 , pentane : EtOAc (1:1)) afforded the product as a beige solid (80.0 mg, 72%). $^1\text{H-NMR}$ (400 MHz, CDCl_3): δ 7.44 - 7.39 (m, 2H), 7.31 - 7.21 (m, 4H), 7.20 - 7.16 (m, 2H), 3.29 (s, 2H) ppm. $^{13}\text{C-NMR}$ (100 MHz, CDCl_3): δ 139.1, 131.9, 130.4, 129.5, 128.8, 125.9 ppm.

Dibenzo[1,2]dithiin



2,2'-Dimercaptobiphenyl (40 mg, 0.18 mmol) and sodium ascorbate (390 mg, 1.97 mmol) were dissolved in CH_3CN (14 mL) and water (9 mL), and stirred for 6 h at rt. The product was then extracted into Et_2O , the organic phase was dried over anhydrous Na_2SO_4 and the solvent removed under reduced pressure. Purification by column chromatography (SiO_2 , pentane : EtOAc (1:1)) afforded the product as a beige solid (30.0 mg, 76%). $^1\text{H-NMR}$ (400 MHz, CDCl_3): δ 7.70 (dd, $J = 7.9, 1.4$ Hz, 2H), 7.52 (dd, $J = 7.6, 1.4$ Hz, 2H), 7.38 (td, $J = 7.6, 1.4$ Hz, 2H), 7.28 (td, $J = 7.5, 1.4$ Hz, 2H) ppm. $^{13}\text{C-NMR}$ (100 MHz, CDCl_3): δ 138.1, 136.3, 129.1, 128.7, 128.0 ppm.

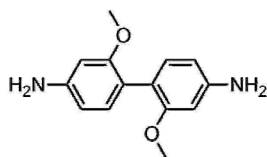
2,2'-Dimethoxy-4,4'-dinitrobiphenyl⁵



A mixture of 4-iodo-3-methoxynitrobenzene (10.1 g, 36.3 mmol) and activated copper powder (9.80 g, 0.15 mol) in dry DMF (40 mL) was stirred at 180 °C for 18 h under a nitrogen atmosphere. The hot suspension was filtered over celite, and the residue was washed with hot DMF. One third of the solvent was removed under reduced pressure, and the remaining filtrate was stored overnight at 4 °C. The precipitate was collected and washed with MeOH. This afforded the product as a pale brown solid (4.23 g, 76%). $^1\text{H-NMR}$ (400 MHz, CDCl_3): δ 7.92 (dd, $J = 8.3, 2.2$ Hz,

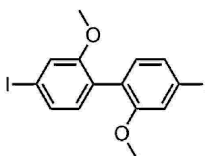
2H), 7.84 (d, $J = 2.2$ Hz, 2H), 7.38 (d, $J = 8.3$ Hz, 2H), 3.88 (s, 6H) ppm. ^{13}C -NMR (100 MHz, CDCl_3): δ 158.2, 146.8, 132.5, 118.34, 107.4 ppm

2,2'-Dimethoxy-4,4'-diaminobiphenyl ⁶



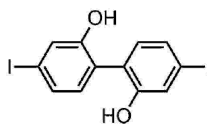
2,2'-Dimethoxy-4,4'-dinitrobiphenyl (4.13 g, 13.6 mmol), tetra-*n*-butylammonium bromide (8.75 g, 27.1 mmol) and sodium sulfide nonahydrate (65.2 g, 0.27 mol) were dissolved in toluene (50 mL) and water (7.0 mL), and the suspension stirred at 95 °C for 16 h. After cooling to rt, the mixture was decanted, the product extracted into toluene, and the combined organic phases washed with water and brine. The organic phase and the separated orange solid were combined and the solvent removed under reduced pressure. Purification by column chromatography (SiO_2 , EtOAc) afforded the product as a yellow solid (2.71 g, 82%). ^1H -NMR (400 MHz, CDCl_3): δ 7.01 (d, $J = 8.2$ Hz, 2H), 6.32 (dd, $J = 8.2, 2.2$ Hz, 2H), 6.31 (d, $J = 2.2$ Hz, 2H), 3.72 (s, 6H), 3.67 (s, 4H) ppm. ^{13}C -NMR (100 MHz, CDCl_3): δ 158.2, 146.8, 132.5, 118.4, 107.2, 99.1 ppm.

2,2'-Dimethoxy-4,4'-diiodobiphenyl ⁷



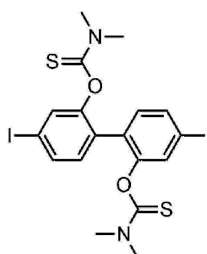
2,2'-Dimethoxy-4,4'-aminobiphenyl (1.13 g, 4.62 mmol) was suspended in CH_3CN (60 mL), and water (60 mL) and concentrated aqueous HCl (20.0 mL, 0.24 mol) were added. The mixture was cooled down to -10 °C, and a 0 °C cold solution of NaNO_2 (1.60 g, 23.2 mmol) in water (8.5 mL) added dropwise. After stirring at rt for 15 min, a 0 °C cold solution of KI (7.68 g, 46.3 mmol) in water (18 mL) was added at -10 °C. After complete addition, the solution was stirred at 80 °C overnight. A saturated aqueous NaHCO_3 solution was then added until pH = 9 was reached. After addition of saturated aqueous $\text{Na}_2\text{S}_2\text{O}_3$ solution, the product was extracted into CH_2Cl_2 . The combined organic phases were washed with brine and dried over anhydrous Na_2SO_4 , and the solvent removed under reduced pressure. Purification by column chromatography (SiO_2 , pentane : EtOAc (10:1)) afforded the product as a white solid (1.87 g, 87%). ^1H -NMR (400 MHz, CDCl_3): δ 7.36 (dd, $J = 7.9, 1.6$ Hz, 2H), 7.29 (d, $J = 1.6$ Hz, 2H), 6.94 (d, $J = 7.9$ Hz, 2H), 3.77 (s, 6H) ppm. ^{13}C -NMR (100 MHz, CDCl_3): δ 157.5, 132.7, 129.8, 126.6, 120.56, 93.7, 56.0 ppm.

4,4'-Diiodo-2,2'-biphenol ⁸



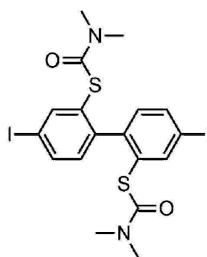
2,2'-Dimethoxy-4,4'-diiodobiphenyl (2.76 g, 5.91 mmol) was dissolved in dry CH₂Cl₂ (45 mL). After slow addition of a solution of BBr₃ in CH₂Cl₂ (1.0 M, 9.5 mL) at -78 °C, the solution was stirred at rt overnight under a nitrogen atmosphere. The mixture was then quenched carefully with aqueous HCl solution (10%) at 0 °C. The product was extracted into Et₂O, the combined organic phases washed with water and dried over anhydrous Na₂SO₄. Removal of the solvent under reduced pressure afforded the product as a pale brown solid (2.51 g, 97%). ¹H-NMR (CDCl₃, 400 MHz): δ 7.41 (d, *J* = 1.7 Hz, 2H) 7.39 (dd, *J* = 7.9, 1.7 Hz, 2H), 6.94 (d, *J* = 7.9 Hz, 2H), 5.43 (s, 2H) ppm.

Dimethylthiocarbamic acid *O*-(2'-dimethylthiocarbamoyloxy-4,4'-di-iodobiphenyl-2-yl)-ester ^{4, 9}



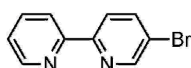
4,4'-Diiodo-2,2'-biphenol (2.97 g, 6.77 mmol) was dissolved in dry DMF (28 mL). NaH (60% in oil, 0.83 mg, 20.8 mmol) was added in small portions at 0 °C, and the mixture stirred for 45 min at rt under a nitrogen atmosphere. Dimethylthiocarbamoyl chloride (3.80 g, 30.7 mmol) was then added, and the solution stirred at 95 °C overnight. After cooling to rt, the mixture was poured into aqueous KOH solution (2%, 50 mL). The white precipitate was filtered off and washed with water. The solid was dissolved in CH₂Cl₂, washed with water, and the solvent removed under reduced pressure. Recrystallization from acetone afforded the product as a pale yellow solid (2.45 g, 53%). ¹H-NMR (CDCl₃, 400 MHz): δ 7.57 (dd, *J* = 8.1, 1.7 Hz, 2H) 7.52 (d, *J* = 1.7 Hz, 2H), 7.11 (d, *J* = 8.1 Hz, 2H), 3.29 (s, 6H), 3.07 (s, 6H) ppm.

Dimethylthiocarbamic acid *S*-(2'-dimethylcarbamoylsulfanyl-4,4'-di-iodobiphenyl-2-yl)-ester ⁹



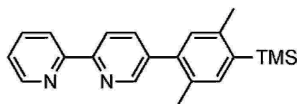
Neat dimethylthiocarbamic acid *O*-(2'-dimethylthiocarbamoyloxy-4,4'-diiodobiphenyl-2-yl)-ester (1.00 g, 1.63 mmol) was heated at 265 °C for 1.5 h under a nitrogen atmosphere. Purification by column chromatography (SiO₂, pentane : EtOAc (2:1)) afforded the product as a pale yellow solid (0.44 g, 44%). ¹H-NMR (CDCl₃, 400 MHz): δ 7.93 (d, *J* = 1.8 Hz, 2H), 7.70 (dd, *J* = 8.1, 1.8 Hz, 2H), 7.00 (d, *J* = 8.1 Hz, 2H), 2.89 (s, 12H) ppm. ¹³C-NMR (CDCl₃, 100 MHz): δ 165.7, 145.1, 144.5, 138.1, 132.2, 130.5, 93.3, 37.1 ppm.

5-Bromo-2,2'-bipyridine ¹⁰



2-Iodo-5-bromopyridine (3.28 g, 11.5 mmol) and Pd(PPh₃)₄ (332 mg, 0.29 mmol) were dissolved in dry THF (20 mL), and 2-pyridylzinc bromide in THF (0.5 M, 30 mL) added. After stirring at 75 °C for 18 h under a nitrogen atmosphere, the mixture was treated with an aqueous solution of EDTA and Na₂CO₃ (0.1 M, 1:1). The product was extracted into CH₂Cl₂ and washed with water. The combined organic phases were dried over anhydrous Na₂SO₄ and the solvent removed under reduced pressure. Purification by column chromatography (SiO₂, pentane : Et₂O (4:1)) afforded the product as a white solid (2.09 g, 77%). ¹H-NMR (400 MHz, CDCl₃): δ 8.72 (dd, *J* = 2.4, 0.7 Hz, 1H), 8.67 (ddd, *J* = 4.8, 1.8, 0.9 Hz, 1H), 8.37 (dt, *J* = 8.0, 1.1 Hz, 1H), 8.32 (dd, *J* = 8.6, 0.7 Hz, 1H), 7.94 (dd, *J* = 8.5, 2.4 Hz, 1H), 7.82 (ddd, *J* = 8.0, 7.5, 1.8 Hz, 1H), 7.33 (ddd, *J* = 7.5, 4.8, 1.2 Hz, 1H) ppm.

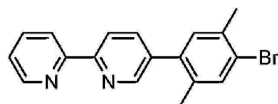
Bpy-xy-TMS ¹¹



5-Bromo-2,2'-bipyridine (1.49 g, 6.34 mmol), 2,5-dimethyl-4-trimethylsilylphenylboronic acid (1.62 g, 7.29 mmol) and Na₂CO₃ (2.02 g, 19.0 mmol) were dissolved in degassed THF (50 mL) and water (50 mL). Pd(PPh₃)₄ (366 mg, 0.32 mmol) was then added, and the mixture stirred for 24 h at 90 °C under a nitrogen atmosphere. After cooling to rt, the product was extracted into CH₂Cl₂, and the organic phase washed with water and brine. The solution was dried over anhydrous Na₂SO₄ and the solvent removed under reduced pressure. Purification by column chromatography

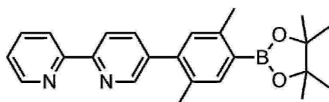
(SiO₂, (i) pentane : EtOAc (4:1), (ii) pentane : EtOAc (2:1)) afforded the product as a white solid (1.96 g, 93%). ¹H NMR (400 MHz, CDCl₃): δ 8.72 (ddd, *J* = 4.9, 1.8, 0.9 Hz, 1H), 8.69 (dd, *J* = 2.3, 0.8 Hz, 1H), 8.49 (dd, *J* = 8.2, 6.5 Hz, 2H), 7.88 (td, *J* = 7.7, 1.8 Hz, 1H), 7.83 (dd, *J* = 8.2, 2.3 Hz, 1H), 7.40 (s, 1H), 7.36 (ddd, *J* = 7.5, 4.8, 1.2 Hz, 1H), 7.09 (d, *J* = 0.9 Hz, 1H), 2.49 (s, 3H), 2.31 (s, 3H), 0.37 (s, 9H) ppm.

Bpy-xy-Br ¹²



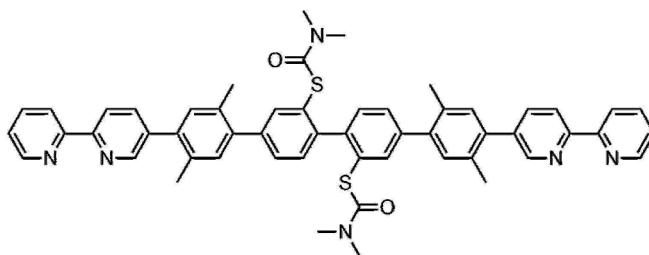
Bpy-xy-TMS (350 mg, 1.05 mmol) and KOAc (206 mg, 2.10 mmol) were dissolved in THF (4.5 mL) and cooled to 0 °C. Br₂ (0.22 mL, 4.29 mmol) was added in the absence of light, and the solution stirred at rt for 2.5 h. After addition of TEA (1.20 mL, 8.65 mmol) and saturated aqueous Na₂S₂O₃ solution, the product was extracted into CH₂Cl₂. The combined organic phases were washed with water and brine, dried over Na₂SO₄, and the solvent removed under reduced pressure. Purification by column chromatography (SiO₂, pentane : Et₂O (6:1)) afforded the product as a colorless viscous oil (314 mg, 88%) ¹H-NMR (400 MHz, CDCl₃): δ 8.71 (ddd, *J* = 4.8, 1.8, 0.9 Hz, 1H), 8.63 (dd, *J* = 2.3, 0.8 Hz, 1H), 8.44 (tt, *J* = 8.0, 1.0 Hz, 2H), 7.84 (td, *J* = 7.8, 1.8 Hz, 1H), 7.76 (dd, *J* = 8.2, 2.3 Hz, 1H), 7.50 (s, 1H), 7.33 (ddd, *J* = 7.5, 4.8, 1.2 Hz, 1H), 7.14 (s, 1H), 2.41 (s, 3H), 2.26 (s, 3H) ppm.

Bpy-xy-bpin



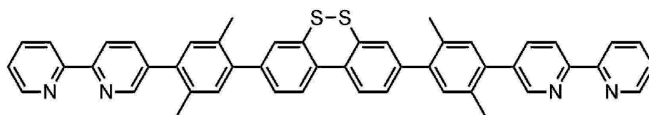
Bpy-xy-Br (314 mg, 0.93 mmol), bis(pinacolato)diboron (361 mg, 1.42 mmol) and KOAc (412 mg, 4.20 mmol) were dissolved in dry and degassed DMF (7 mL), and Pd(PPh₃)₄ (65 mg, 0.09 mmol) added. The mixture was stirred at 120 °C for 17 h under a nitrogen atmosphere, and after cooling to rt, saturated aqueous NH₄Cl solution was added. The resulting suspension was extracted with CH₂Cl₂. The combined organic phases were washed with water and brine, dried over anhydrous Na₂SO₄, and the solvent removed under reduced pressure. Purification by column chromatography (SiO₂, pentane : Et₂O (3:1)) afforded the product as a colourless, strongly viscous oil (317 mg, 88%). ¹H NMR (400 MHz, CDCl₃): δ 8.60 (ddd, *J* = 4.9, 1.8, 0.9 Hz, 1H), 8.57 (dd, *J* = 2.3, 0.9 Hz, 1H), 8.35 (tt, *J* = 7.0, 1.0 Hz, 2H), 7.77 - 7.66 (m, 2H), 7.64 (s, 1H), 7.21 (ddd, *J* = 7.5, 4.8, 1.2 Hz, 1H), 7.01 (s, 1H), 2.47 (s, 3H), 2.20 (s, 3H), 1.26 (s, 12H) ppm.

Protected Ligand

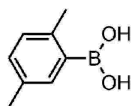


Bpy-xy-bpin (154 mg, 0.39 mmol), dimethylthiocarbamic acid *S*-(2'-dimethyl-carbamoyl-sulfanyl-4,4'-diiodobiphenyl-2-yl) ester (100 mg, 0.17 mmol) and Na₂CO₃ (408 mg, 3.85 mmol) were dissolved in degassed THF (7 mL) and water (2.4 mL). Pd(PPh₃)₄ (18.8 mg, 0.02 mmol) was added, and the mixture was stirred at 85 °C for 22 h under a nitrogen atmosphere. After cooling to rt, the product was extracted into CH₂Cl₂, and the combined organic phases washed with water and brine. The organic phase was dried over anhydrous Na₂SO₄, and the solvent was removed under reduced pressure. Purification by column chromatography (SiO₂, Et₂O : TEA (100:1)) afforded the product as a slightly yellow solid (34.9 mg, 24%). ¹H-NMR (400 MHz, CDCl₃): δ 8.75 - 8.69 (m, 4H), 8.47 (ddd, *J* = 9.8, 8.1, 1.0 Hz, 4H), 7.87 (ddd, *J* = 7.7, 5.7, 2.0 Hz, 4H), 7.68 (t, *J* = 1.2 Hz, 2H), 7.47 - 7.42 (m, 4H), 7.36 - 7.31 (m, 4H), 7.22 (s, 2H), 2.93 (s, 12H), 2.41 (s, 6H), 2.35 (s, 6H) ppm.

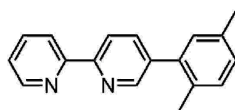
Ligand



The protected ligand (34.9 mg, 0.04 mmol) was dissolved in degassed THF (3 mL) and CH₃OH (3 mL), and NaOH (40 mg, 1.0 mmol) added. After stirring for 2 h at 80 °C under a nitrogen atmosphere, the mixture was cooled to rt. Water was added and the solution neutralized with diluted aqueous HCl solution. Afterwards, the product was extracted into CH₂Cl₂, and the combined organic phases washed with water and brine. The organic phase was dried over anhydrous Na₂SO₄, and the solvent removed under reduced pressure. The crude product was purified by column chromatography (SiO₂, Et₂O : triethylamine (100:1)), affording a mixture of the disulfide and dithiol species. Stirring of the mixture in CH₂Cl₂ under air, followed by removal of the solvent, afforded the product as a slightly yellow solid (10 mg, 34%). ¹H-NMR (400 MHz, CDCl₃): δ 8.76 - 8.70 (m, 4H), 8.53 - 8.42 (m, 4H), 7.90 - 7.80 (m, 6H), 7.57 (d, *J* = 1.8 Hz, 2H), 7.43 (dd, *J* = 8.0, 1.8 Hz, 2H), 7.34 (ddd, *J* = 7.6, 4.8, 1.2 Hz, 2H), 7.27 (s, 2H), 7.24 (s, 2H) 2.38 (s, 6H), 2.36 (s, 6H) ppm. MS (ESI) calcd for H₃₇C₄₈N₄S₂ ([M+H]⁺): *m/z* 733.25. Found: *m/z* 733.20.

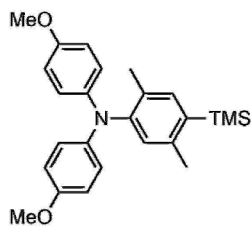
Xy-B(OH)₂¹³

Magnesium turnings (77.0 mg, 3.17 mmol) were suspended in dry THF (1 mL), and a solution of 2,5-dimethylbromobenzene (536 mg, 0.4 mL, 2.90 mmol) in dry THF (4 mL) added dropwise. The mixture was heated to reflux for 3.5 h under a nitrogen atmosphere. After cooling to -78 °C, boric acid (366 mg, 0.40 mL, 3.52 mmol) was added, and the reaction mixture stirred for 2.5 d at rt. Aqueous HCl solution (2 M, 5 mL) was then added slowly, and the solution stirred for 20 min. The product was extracted into Et₂O, and the combined organic phases washed with water and brine. The organic phase was dried over anhydrous Na₂SO₄, and the solvent removed under reduced pressure. Purification by column chromatography (SiO₂, CH₂Cl₂ : pentane (2:1) → EtOAc → EtOAc : MeOH (90:10)) afforded the product as a white solid (300 mg, 69%). ¹H-NMR (400 MHz, CDCl₃): δ 8.00 (dd, *J* = 2.0, 0.9 Hz, 1H), 7.26 (s, 1H), 7.17 (d, *J* = 7.7 Hz, 1H), 2.77 (s, 3H), 2.39 (d, *J* = 1.0 Hz, 3H) ppm. ¹³C-NMR (100 MHz, CDCl₃): □ 164.8, 156.8, 151.1, 150.0, 125.0, 124.4, 37.0 ppm.

Bpy-xy-H¹⁴

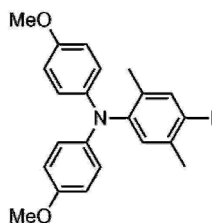
5-Bromo-2,2'-bipyridine (251 mg, 1.07 mmol), xy-B(OH)₂ (184 mg, 1.15 mmol) and Na₂CO₃ (380 mg, 3.58 mmol) were dissolved in degassed THF (8 mL) and water (8 mL). Pd(PPh₃)₄ (62.0 mg, 0.05 mmol) was then added, and the mixture was stirred at 90 °C for 20 h under a nitrogen atmosphere. After cooling to rt, the product was extracted into CH₂Cl₂, the combined organic phases washed with water and brine. The organic phase was dried over anhydrous Na₂SO₄, and the solvent removed under reduced pressure. Purification by column chromatography (SiO₂, pentane : Et₂O (4:1)) afforded the product as a yellow oil (238 mg, 86%). ¹H-NMR (400 MHz, CDCl₃): δ 8.73 (ddd, *J* = 4.8, 1.8, 0.9 Hz, 1H), 8.69 (dd, *J* = 2.3, 0.9 Hz, 1H), 8.50 - 8.45 (m, 2H), 7.86 (td, *J* = 7.8, 1.8 Hz, 1H), 7.82 (dd, *J* = 8.1, 2.3 Hz, 1H), 7.35 (ddd, *J* = 7.5, 4.8, 1.2 Hz, 1H), 7.24 (d, *J* = 7.7 Hz, 1H), 7.19 - 7.14 (m, 1H), 7.13 (d, *J* = 1.7 Hz, 1H), 2.40 (d, *J* = 0.9 Hz, 3H), 2.31 (s, 3H) ppm. ¹³C-NMR (100 MHz, CDCl₃): δ 156.2, 154.7, 149.5, 149.4, 138.0, 137.8, 137.6, 137.1, 135.8, 132.7, 130.7, 130.7, 129.0, 123.8, 121.2, 120.6, 21.1, 20.1 ppm.

TAA-TMS¹⁴



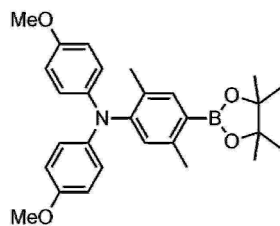
4,4'-Dimethoxydiphenylamine (1.16 g, 5.06 mmol), Br-xy-TMS (1.43 g, 5.56 mmol), potassium *tert*-butoxide (1.69 g, 15.1 mmol), tri-*tert*-butyl-phosphonium tetrafluoroborate (79.0 mg, 0.25 mmol) and Pd(dba)₂ (160 mg, 0.28 mmol) were dissolved in dry and degassed toluene (25 mL), and stirred for 17 h at 90 °C under a nitrogen atmosphere. After cooling to rt, the mixture was diluted with water (100 mL) and the product extracted into CH₂Cl₂. The organic solution was dried over anhydrous Na₂SO₄, and the solvent removed under reduced pressure. Purification by column chromatography (SiO₂, pentane : EtOAc (10:1)) afforded the product as a white solid (1.81 g, 88%). ¹H-NMR (250 MHz, CDCl₃): δ 7.25 (s, 1H), 6.91 - 6.82 (m, 5H), 6.80 - 6.68 (m, 4H), 3.76 (s, 6H), 2.33 (s, 3H), 1.97 (s, 3H), 0.33 (s, 9H) ppm.

TAA-I¹⁴



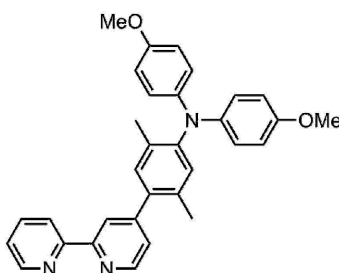
TAA-TMS (1.81 g, 4.46 mmol) was dissolved in dry CH₂Cl₂ (30 mL). After cooling to -78 °C, iodine monochloride (1.45 g, 0.46 mL, 9.01 mmol) in dry CH₂Cl₂ (10 mL) was added dropwise. The mixture was stirred at -78 °C for 10 min under a nitrogen atmosphere, then aqueous Na₂S₂O₃ solution was added. After warming to rt, the product was extracted into CH₂Cl₂. The combined organic phases were then dried over anhydrous Na₂SO₄, and the solvent removed under reduced pressure. Purification by column chromatography (SiO₂, pentane : CH₂Cl₂ (1:1)) afforded the product as a white solid (1.78 g, 87%). ¹H-NMR (400 MHz, CDCl₃): δ 7.63 (s, 1H), 7.14 - 6.37 (m, 9H), 3.78 (s, 6H), 2.29 (s, 3H), 1.91 (s, 3H) ppm.

TAA-bpin¹⁴



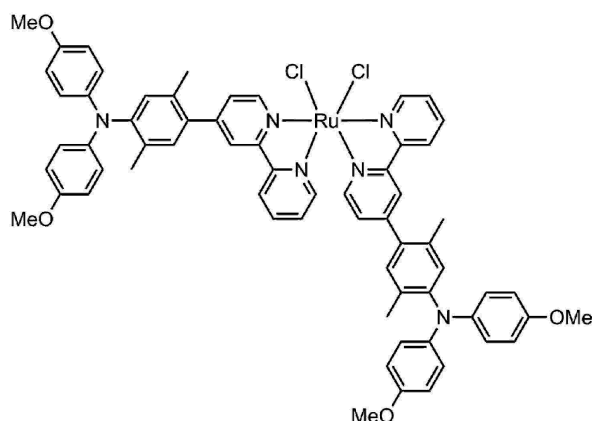
TAA-I (1.59 g, 3.46 mmol), bis(pinacolato)diboron (1.53 g, 6.03 mmol) and KOAc (1.53 g, 15.5 mmol) were dissolved in dry and degassed DMSO (20 mL), before Pd(PPh₃)₂Cl₂ (140 mg, 0.12 mmol) was added. The mixture was stirred for 20.5 h at 90 °C under a nitrogen atmosphere. After cooling to rt, saturated, aqueous NH₄Cl solution and water were added. The product was extracted into Et₂O, the combined organic phases dried over anhydrous Na₂SO₄, and the solvent removed under reduced pressure. Purification by column chromatography (SiO₂, pentane : EtOAc (10:1)) afforded the product as a slightly yellow solid (1.47 g, 84%). ¹H-NMR (400 MHz, CDCl₃): δ 7.58 (s, 1H), 7.85 - 7.82 (m, 5H), 6.78 - 6.70 (m, 4H), 3.77 (s, 6H), 2.40 (s, 3H), 1.93 (s, 3H), 1.34 (s, 12H) ppm.

4-TAA-bpy



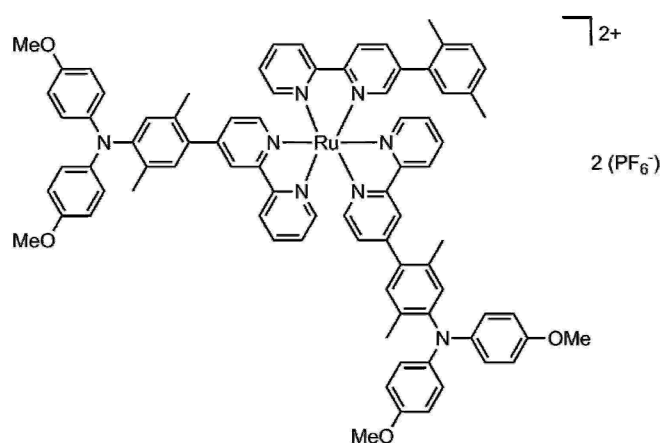
4-Bromo-2,2'-bipyridine (410 mg, 1.74 mmol), TAA-bpin (800 mg, 1.74 mmol) and Na₂CO₃ (1.87 g, 17.7 mmol) were dissolved in degassed water (8 mL) and THF (32 mL). After addition of Pd(PPh₃)₄ (190 mg, 0.16 mmol), the solution was stirred at 85 °C for 23 h under a nitrogen atmosphere. After cooling to rt, the product was extracted into CH₂Cl₂, and the organic phase washed with water and brine. The organic phase was dried over anhydrous Na₂SO₄, and the solvent removed under reduced pressure. Purification by column chromatography (SiO₂, pentane : EtOAc (4:1) → EtOAc) afforded the product as a yellow solid (771 mg, 90%). ¹H-NMR (400 MHz, CDCl₃): δ 8.80 - 8.70 (m, 3H), 8.57 (s, 1H), 7.94 (t, *J* = 7.9 Hz, 1H), 7.49 (s, 1H), 7.41 (t, *J* = 6.2 Hz, 1H), 7.17 (s, 1H), 6.97 (s, 1H), 6.95 - 6.86 (m, 4H), 6.85 - 6.75 (m, 4H), 3.79 (s, 6H), 2.25 (s, 3H), 1.99 (s, 3H) ppm.

Ru(4-TAA-bpy)₂Cl₂



Ru(DMSO)₄Cl₂ (114 mg, 0.23 mmol), 4-TAA-bpy (227 mg, 0.47 mmol) and LiCl (40 mg, 0.94 mmol) were dissolved in dry DMF (14 mL), and the solution stirred for 90 min at 170 °C under a nitrogen atmosphere, before the solvent was removed under reduced pressure. Purification by column chromatography (SiO₂, (i) acetone, (ii) CH₂Cl₂ : CH₃OH (50:3, v:v), (iii) CH₂Cl₂ : CH₃OH (9:1, v:v)) afforded the product as a dark violet solid (30 mg, 11%). MS (ESI) calcd for C₆₄H₅₈N₆O₄ClRu ([M-Cl]⁺): *m/z* 1111.33. Found: *m/z* 111.41.

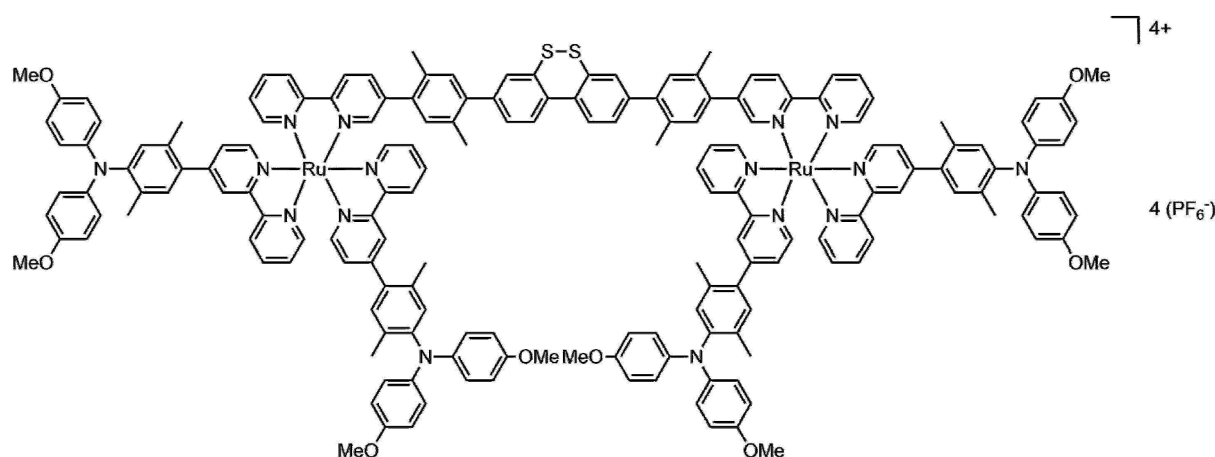
TAA-Ru



Ru(4-TAA-bpy)₂Cl₂ (23.0 mg, 0.02 mmol) and bpy-xy-H (5.5 mg, 0.02 mmol) were dissolved in EtOH (0.5 mL) and CH₂Cl₂ (1.5 mL), and stirred for 18 h at 100 °C under a nitrogen atmosphere, before the solvent was removed under reduced pressure. The crude product was purified by column chromatography (SiO₂, acetone → acetone : water (90:10) → acetone : water : sat. aqueous KNO₃ (95:4:1)). After removal of the organic solvent under reduced pressure, the complex was precipitated by adding saturated aqueous KPF₆ solution. The solid was filtered off, and washed with water and Et₂O, affording the product as a red solid (13 mg, 40%). ¹H-NMR (400 MHz, acetonitrile-*d*₃): δ 8.64 - 8.52 (m, 4H), 8.50 (dd, *J* = 6.4, 1.9 Hz, 2H), 8.13 - 8.05 (m, 3H), 8.01 (td, *J* = 7.9, 1.5 Hz, 1H), 7.93 - 7.86 (m, 1H), 7.88 - 7.77 (m, 3H), 7.76 (d, *J* = 5.9 Hz, 1H), 7.65 (dd, *J* = 2.0, 0.7 Hz, 1H), 7.50 - 7.35 (m, 5H), 7.27 (d, *J* = 8.1 Hz, 2H), 7.13 (d, *J* = 1.2 Hz, 2H), 6.99 (d, *J* = 2.2 Hz, 3H), 6.84 (d, *J* = 1.0 Hz, 16H), 3.75 (s, 12H), 2.25 (s, 3H), 2.23 (s, 3H), 2.15 (s, 6H), 2.01 (s, 6H) ppm. HRMS (ESI) calcd for C₈₂H₇₄N₈O₄Ru ([M-2(PF₆⁻)]²⁺): *m/z* 669.2444. Found *m/z*

668.2442. Elemental analysis calcd for $C_{82}H_{74}F_{12}N_8O_4P_2Ru \cdot 1.5 H_2O$: C, 59.56; H, 4.69; N, 6.78. Found: C, 59.39; H, 4.80; N, 7.03.

Heptad



$Ru(4-TAA-bpy)_2Cl_2$ (28.2 mg, 0.02 mmol) and the ligand (9.00 mg, 0.01 mmol) were dissolved in EtOH (0.8 mL) and CH_2Cl_2 (2.4 mL), and stirred for 48 h at 100 °C under a nitrogen atmosphere, before the solvent was removed under reduced pressure. The crude product was purified by column chromatography (SiO_2 , acetone \rightarrow acetone : water (90:10) \rightarrow acetone : water : sat. aqueous KNO_3 (95:4:1)). After removal of the organic solvent under reduced pressure, the complex was precipitated by adding saturated aqueous KPF_6 solution. Filtration, followed by washing with water and Et₂O afforded the product as a red solid (11.4 mg, 27%). 1H -NMR (400 MHz, acetone- d_6): δ 9.05 (dt, $J = 8.1, 1.6$ Hz, 4H), 8.99 - 8.90 (m, 4H), 8.89 (dt, $J = 3.8, 1.6$ Hz, 4H), 8.35 - 8.12 (m, 18H), 8.10 (d, $J = 1.8$ Hz, 2H), 7.97 (d, $J = 8.1$ Hz, 2H), 7.72 - 7.55 (m, 10H), 7.54 (d, $J = 1.8$ Hz, 2H), 7.47 (dd, $J = 8.1, 1.9$ Hz, 2H), 7.30 (d, $J = 5.5$ Hz, 4H), 7.22 (d, $J = 3.8$ Hz, 4H), 7.00 (s, 4H), 6.86 (d, $J = 1.6$ Hz, 32H), 3.77 (s, 12H), 3.77 (s, 12H), 2.27 (s, 12H), 2.14 (s, 6H), 2.09 (s, 6H), 2.00 (s, 12H) ppm. HRMS (ESI) calcd $C_{176}H_{152}N_{16}O_8Ru_2S_2$ for $[M-4(PF_6^-)]^{4+}$: m/z 721.4887. Found: m/z 721.4899. Elemental analysis calcd for $C_{176}H_{152}F_{24}N_{16}O_8P_4Ru_2S_2 \cdot 8 H_2O$: C, 58.57; H, 4.69; N, 6.21. Found: C, 58.57; H, 4.77; N, 6.07.

The synthesis of $[Ru(L^1)_2(L^2)]^{2+}$ complexes is somewhat more straightforward than the synthesis of $[Ru(L^1)(L^2)(L^3)]^{2+}$ complexes (where L^1 , L^2 , L^3 are bidentate chelating ligands). This is the reason for including two TAA units per photosensitizer unit.

The molar extinction coefficients (ϵ) at the MLCT (ca. 450 nm) and π - π^* absorption maxima (ca. 290 nm) are approximately twice as high in the heptad (red trace) than in the TAA-Ru reference compound (grey trace) because the heptad has two Ru(bpy)₃²⁺ chromophores (Figure S1a). However, the most important difference between the two spectra is the appearance of an additional shoulder at 330 nm in the heptad spectrum. This shoulder is attributed to an absorption caused by the dibenzo[1,2]dithiin (PhSSPh) acceptor, as confirmed by the absorption spectrum of the free bpy-xy-PhSSSPH-xy-bpy ligand in CH₂Cl₂ (Figure S1b). Disappearance of this absorption band upon two-electron reduction (see SI page S19, S20) is the key spectroscopic observable for the light-driven accumulation of reduction equivalents by transient absorption spectroscopy (Figure 1 of the main paper).

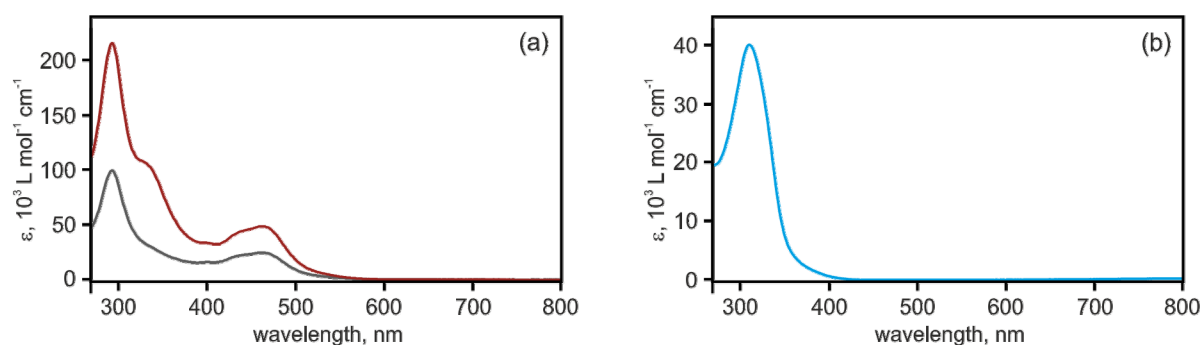


Figure S1. (a) Optical absorption spectra of the heptad (red) and TAA-ref (grey) in dry CH₃CN at 22 °C. (b) Absorption spectrum of the bpy-xy-PhSSSPH-xy-bpy ligand in CH₂Cl₂ at 22 °C.

The absorption spectrum of the free ligand with two bpy and *p*-xylene units attached covalently to a central PhSSPh unit (Figure 1b) shows an absorption band at 310 nm with $\epsilon = 40'000 \text{ l mol}^{-1} \text{ cm}^{-1}$. For solubility reasons, this spectrum was measured in CH₂Cl₂, and this may be one of the reasons why this band is slightly shifted relative to the shoulder observed in the heptad spectrum (310 nm instead of 330 nm). The UV-Vis absorption data reported here are in line with a prior study of a PhSSPh compound.⁹

The PhSSPh reference compound (see Scheme 1b in the main paper for molecular structure) exhibits the typical features of redox potential inversion as reported previously for the same compound substituted with two peripheral iodine atoms.⁹ Specifically, there is a difference of more than 1.0 Volt between oxidative and reductive peak potentials for corresponding two-electron half-waves, and there is a significant dependence on potential sweep rate of both peak potentials and currents (Figure S2a). The prior study revealed linear correlation of the peak potentials with the natural logarithm of the scan rate and the peak current with the square root of the scan rate,⁹ and this is also the case for our PhSSPh reference compound (Figure S2b, S2c).

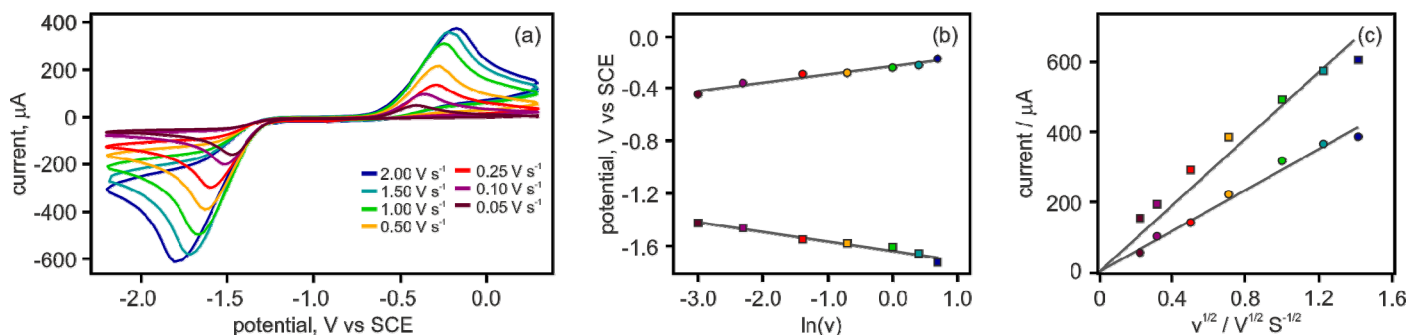
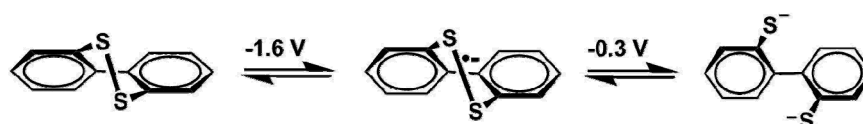


Figure S2. (a) Cyclic voltammograms of the PhSSPh reference compound (5.1 mM) in dry, de-aerated CH₃CN containing 0.1 M TBAPF₆ as supporting electrolyte. Potential sweep rates are indicated in the inset. (b) Plot of peak potentials versus the natural logarithm of the scan rate. (c) Plot of peak currents versus the square root of the sweep rate.

On cathodic scans, the peak potentials vary from -1.78 to -1.47 V vs. SCE and on return (anodic) scans from -0.45 to -0.17 V vs. SCE. The potentials reported in the main paper (-1.6 and -0.3 V vs. SCE, respectively) are average values. The reduction of the disulfide is a stepwise two-electron process according to prior studies.^{3, 9, 15} The radical monoanion exhibits an elongated S-S bond due to the population of a σ^* orbital with an extra electron, but the S-S bond remains intact (Scheme S1). Upon further reduction with a second electron, the S-S bond cleaves and the thiolate groups rotate away from each other to minimize electrostatic repulsion. The thermodynamic stabilization associated with that structural reorganization process is the main origin of the redox potential inversion. The entire process is reversed upon application of an oxidative potential.



Scheme S1. Structural changes upon reduction of the PhSSPh unit. Potentials are given in V vs. SCE.

In presence of sufficiently strong acid, two-electron reduction of PhSSPh is expected to result in the corresponding dithiol compound (PhSHPhSH). Cyclic voltammetry of the PhSSPh reference compound in presence of *p*-toluenesulfonic acid (TsOH) is in line with this expectation (Figure S3). Increasing the concentration of TsOH up to 5.2 equivalents does not affect the two-electron reduction potential of the disulfide significantly. Only a shift of ca. 50 mV to less negative values is detected in that range. By contrast, the peak for two-electron return oxidation observed at -0.3 V vs. SCE in neat CH₃CN disappears upon addition of TsOH. Instead, two new irreversible oxidation waves with peaks at 1.56 and 1.82 V vs. SCE appear when measuring the PhSHPhSH reference compound (Figure S3, right), and they are tentatively assigned to consecutive single-electron oxidation of the two individual thiol moieties.

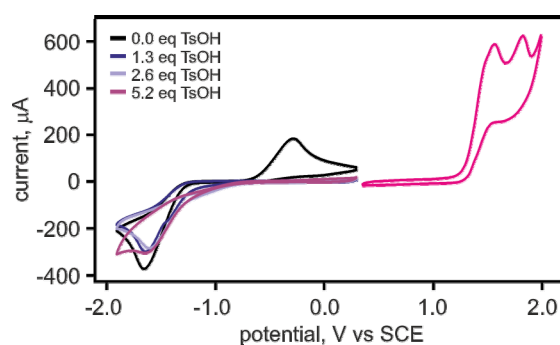


Figure S3. Cyclic voltammograms of the PhSSPh reference compound (6.0 mM, left) in dry, de-aerated CH₃CN in the presence of increasing TsOH concentrations (inset) and of the PhSHPhSH reference compound (6.0 mM, right). 0.1 M TBAPF₆ was the supporting electrolyte. The potential sweep rate was 0.5 V/s.

The cyclic voltammograms of the TAA-Ru reference compound (upper part of Figure S4) is essentially a superposition of all redox waves expected for the Ru(bpy)₃²⁺ complex combined with the one-electron oxidation of TAA. All potentials for bpy-related reductions, metal-centered oxidation, and TAA-based oxidation processes are in line with the known potentials of the respective isolated components when not linked covalently to one another.¹⁶ The voltammogram of the heptad (lower part of Figure S4) is of somewhat lower quality due to the small amount of available substance.⁹ While all Ru(bpy)₃²⁺-related and TAA-related redox processes are still detectable in satisfactory manner, the PhSSPh-related redox processes are more difficult to identify unambiguously. We therefore rely on the cyclic voltammogram of the PhSSPh reference compound (Figure S2a) for the acceptor potentials. Table S1 summarizes all relevant redox potentials of the individual components in the molecular heptad. Potentials for the ³MLCT-excited photosensitizer unit were estimated based on the ground-state redox processes and an MLCT energy of 2.1 eV.^{16a}

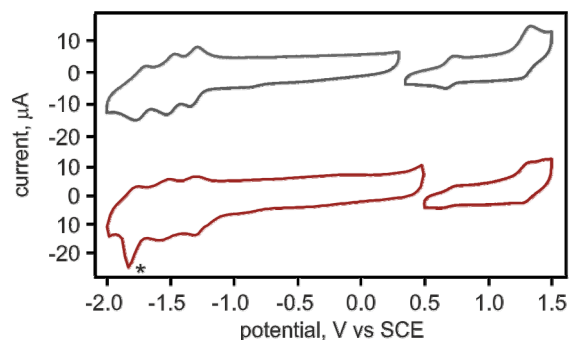


Figure S4. Cyclic voltammograms of the TAA-Ru reference compound (grey trace, 83 μM) and the molecular heptad (red trace, 39 μM) in dry, de-aerated CH₃CN with 0.1 M TBAPF₆. Oxidative and reductive sweeps were measured separately to obtain voltammograms of higher quality. The potential sweep rate was 0.5 V/s. The asterisk denotes a peak resulting from adsorption of the compound on the working electrode surface.

Table S1. Redox potentials (in V vs. SCE) for the donor, acceptor, and sensitizer units in the molecular heptad.

redox couple		redox couple	
PhSSPh / PhSSPh ⁻	-1.6	Ru(bpy) ₃ ²⁺ / Ru(bpy) ₃ ⁺	-1.3
PhSSPh ⁻ / PhS ⁻ PhS ⁻	-0.3	Ru(bpy) ₃ ³⁺ / Ru(bpy) ₃ ²⁺	1.3
TAA ⁺ / TAA	0.7	*Ru(bpy) ₃ ²⁺ / Ru(bpy) ₃ ⁺	0.8
		Ru(bpy) ₃ ³⁺ / *Ru(bpy) ₃ ²⁺	-0.8

^a Measured in dry Ar-purged CH₃CN at 22 °C with scan rates of 0.5 V/s. Relevant data are shown in Figures S2a and S4.

The UV-Vis difference spectrum of the bpy-xy-PhSSPh-xy-bpy ligand in dry, de-aerated CH_2Cl_2 was obtained by measuring the optical absorption spectrum of a 99 μM solution before and after applying a potential of -2.0 V vs. SCE (Figure S5). The first bpy-localized reduction in the free ligand occurs at -2.2 V vs. SCE,¹⁷ while PhSSPh reduction already sets in at -1.6 V vs. SCE. Consequently, when applying a potential of -2.0 V vs. SCE one expects selective reduction of the PhSSPh unit. The key observation is a bleach of the π - π^* absorption at 330 nm and an increase in absorption at 285 nm (Figure S5). Upon two-electron reduction, the disulfide bond is cleaved (Scheme S1), and the thiolate groups rotate away from each other, leading decreased π -conjugation and the observable hypsochromic shift of a π - π^* absorption band when going from PhSSPh to PhS^-PhS^- .

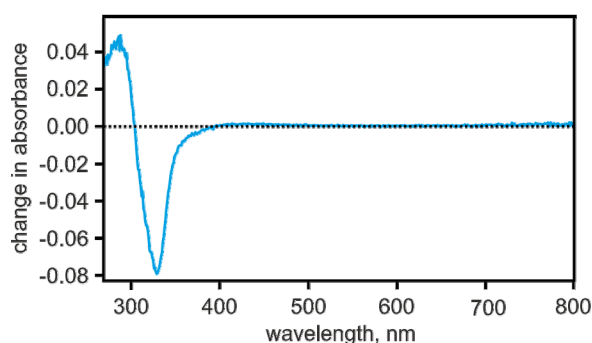


Figure S5. UV-Vis difference spectrum obtained after reduction of the bpy-xy-PhSSPh-xy-bpy ligand (99 μM) in dry, de-aerated CH_2Cl_2 containing 0.1 M TBAPF₆. The applied potential was -2.0 V vs. SCE.

The spectrum of the PhSSPh^- monoanion is not accessible by spectro-electrochemistry, because one-electron reduction cannot be achieved electrochemically. However, the PhSSPh^- species has an intact disulfide bond and a similar degree of π -conjugation between the two adjacent phenyls as the PhSSPh parent species, and consequently the absorption band at 330 nm is expected to be less affected by one-electron reduction than by two-electron reduction.

UV-Vis difference spectra of the TAA-Ru reference compound (Figure S6a) and the heptad (Figure S6b) provide further evidence for the fact that a bleach at 330 nm is a diagnostic spectral feature for the reduction of the PhSSPh acceptor to PhS^-PhS^- . Reduction of TAA-Ru at potentials of -1.4 and -1.6 V vs. SCE leads to absorption bands around 375 and 520 nm which are typical for π - π^* transitions of a reduced bpy ligand of the photosensitizer.¹⁸ In addition, a bleach of the bpy-based π - π^* absorption at 290 nm and an MLCT ground state absorption bleach are detected at 455 nm (Figure S6a). For the heptad, the same spectral changes are observed upon reduction (bands at 290, 375, 520 nm, bleach at 455 nm), but there is an additional bleach at 330 nm caused by the two-electron reduction of the PhSSPh acceptor unit, in line with the data in Figure S5.

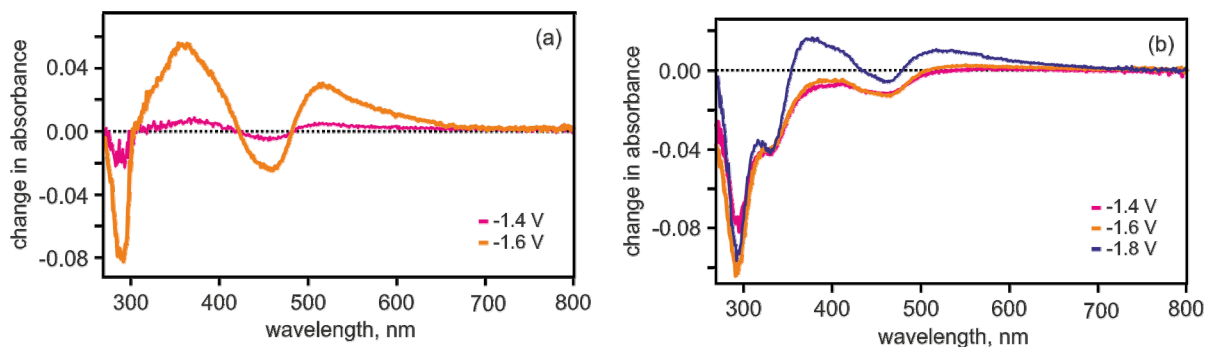


Figure S6. UV-Vis difference spectra obtained after reduction of (a) the TAA-Ru reference compound (80 μM) and (b) the heptad (37 μM) in dry, de-aerated CH₃CN containing 0.1 M TBAPF₆. Applied potentials are given V vs. SCE.

The spectral features of TAA⁺ are in principle well known,^{16b, c} yet we measured them specifically for the TAA-Ru reference compound (grey trace) and the molecular heptad (red trace in Figure S7). As expected, one observes absorption bands at 375 and 775 nm, as well as bleaches around 290 and 455 nm following one-electron oxidation at a potential of 1.0 V vs. SCE.

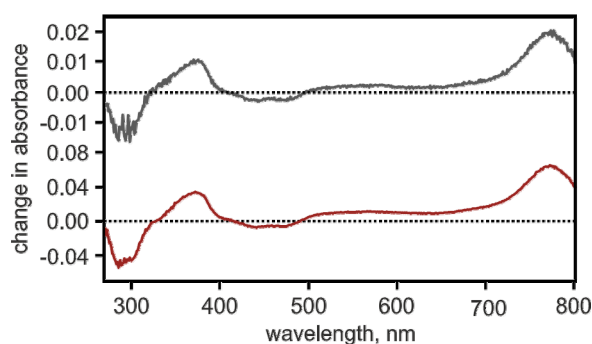
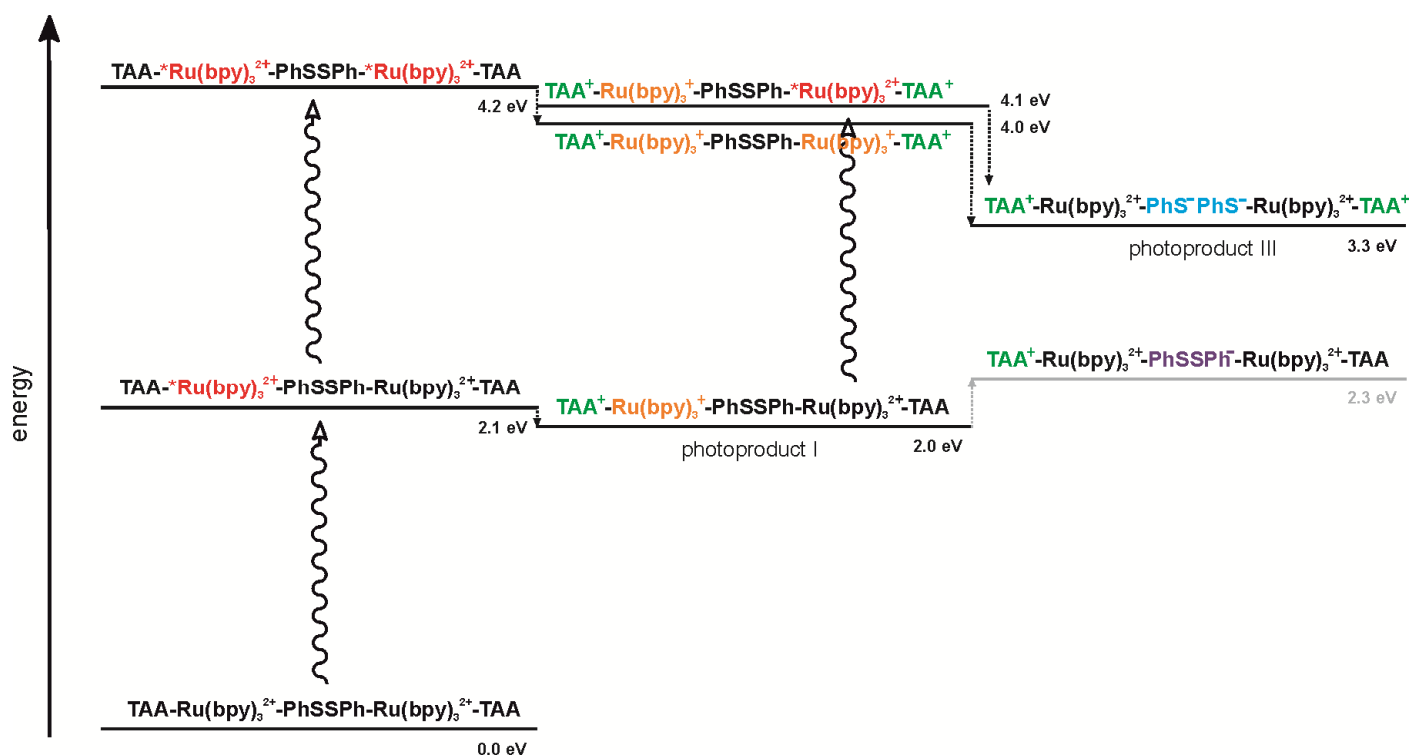


Figure S7. UV-Vis difference spectra obtained after oxidation of the TAA-Ru reference compound (grey trace, 90 μM) and the heptad (red trace, 37 μM) in dry, de-aerated CH₃CN containing 0.1 M TBAPF₆. A potential of 1.0 V vs. SCE was applied in both cases.

Energy-level scheme

Based on the redox potentials in Table S1, an energy level scheme can be established (Scheme S2). The respective scheme illustrates possible reaction pathways to the **TAA⁺-Ru(bpy)₃²⁺-PhS[•]PhS⁻-Ru(bpy)₃²⁺-TAA⁺** key photoproduct (no. III in Table S2). The lowest ³MLCT excited state of Ru(bpy)₃²⁺ is 2.1 eV above the ground state.^{16a} Reductive ³MLCT quenching by TAA is exergonic by 0.1 eV based on the data in Table S1, leading to an energy of ca. 2.0 eV for the **TAA⁺-Ru(bpy)₃⁺-PhSSPh-Ru(bpy)₃²⁺-TAA** photoproduct (no. I in Table S2). Reduction of the disulfide PhSSPh to its radical monoanionic form (PhSSPh^{•-}) requires a potential of -1.6 V vs. SCE (Table S1), and consequently the hypothetical product **TAA⁺-Ru(bpy)₃²⁺-PhSSPh^{•-}-Ru(bpy)₃²⁺-TAA** would have an energy of 2.3 eV. There is no spectroscopic evidence for this product and given that its formation is endergonic by 0.3 eV from the initially formed photoproduct I, we assume that this hypothetical intermediate does not play an important role. (Oxidative quenching of ³MLCT-excited Ru(bpy)₃²⁺ to form PhSSPh^{•-} is thermodynamically similarly unfavorable; the respective photoproduct is not shown in Scheme S2).



Scheme S2. Energy level scheme for the molecular heptad based on the redox potentials in Table S1.

Excitation of both Ru(bpy)₃²⁺ photosensitizer units on a given heptad can lead to the formation of two TAA⁺ / Ru(bpy)₃⁺ pairs within the same molecule, and the respective **TAA⁺-Ru(bpy)₃⁺-PhSSPh-Ru(bpy)₃⁺-TAA⁺** photoproduct is expected to store 4.0 eV. Alternatively, the formation of photoproduct I (**TAA⁺-Ru(bpy)₃⁺-PhSSPh-Ru(bpy)₃²⁺-TAA** state at 2.0 eV) can occur prior to excitation of the second photosensitizer unit. This pathway leads to the **TAA⁺-Ru(bpy)₃⁺-PhSSPh*-Ru(bpy)₃²⁺-TAA** intermediate at 4.1 eV and seems very plausible.

The side product **TAA⁺-Ru(bpy)₃²⁺-PhSSPh-Ru(bpy)₃⁺-TAA** (no. II in Table S2) has essentially the same energy as product I. Possible reaction pathways leading to its formation are discussed in the following section.

Of key interest in the transient absorption studies was the spectral range around 320 nm where the reduction of the PhSSPh acceptor leads to a diagnostic bleach according to the detailed spectro-electrochemical studies presented above (Figures S5-S6). Due to the high molar extinction of the heptad in this spectral range (red trace in Figure S1a), very dilute solutions (below 5 μ M) had to be investigated, and this made the acquisition of high-quality data with good signal-to-noise ratio very challenging. Use of a beam expander from THORLABS was crucially important to optimize the spatial overlap between pump and probe beams in the LP920-KS spectrometer. The beam expander was used for the laser pump beam because the lamp probe beam was significantly larger. Nevertheless, excitation power dependent measurements of the bleach at 320 nm were not possible. In principle, one would expect a quadratic dependence of this bleach on excitation power because this signal is the result of a two-photon process.¹⁹

In the main paper, the transient absorption spectrum obtained from the heptad in neat CH₃CN (Figure 1a) is compared to spectro-electrochemical data obtained from the free bpy-xy-PhSSPh-xy-bpy ligand (Figure 1d; molecular structure shown in Scheme 1d) in order to identify the two-electron reduction product PhS⁻PhS⁻ at the central acceptor unit. Additionally, the transient absorption spectrum can also be compared to spectro-electrochemical data obtained directly from the heptad molecule to further corroborate the interpretation of the respective time-resolved data (Figure S8). Toward this end, the transient absorption spectrum from Figure 1a and the TAA⁺/TAA difference spectrum from Figure 1b are reproduced in Figure S8a/b (black and green traces, respectively). The spectro-electrochemical UV-Vis difference spectrum obtained from the heptad in de-aerated CH₃CN after applying a potential of -1.8 V vs. SCE clearly shows the anticipated bleach at 330 nm due to disulfide reduction (Figure S8c, reproduced from Figure S6b). In addition, there is a negative signal at ca. 290 nm caused by reduction of a bpy ligand. The red spectrum shown in Figure S8d is the same as that in Figure 1d of the main paper, resulting from subtraction of the TAA⁺ contribution (green trace in Figure S8b / Figure 1b) from the transient absorption spectrum (black trace in Figure S8a / Figure 1a). For this subtraction, the TAA⁺/TAA difference spectrum was scaled such that the change in absorbance at 775 nm matches that observed in the transient absorption spectrum. The resulting derived spectrum shows the spectral contribution of the reduction products Ru(bpy)₃⁺ (bands at 375, 520 nm, bleach at 455 nm) and PhS⁻PhS⁻ (bleach at 320 nm), as discussed in the main paper.

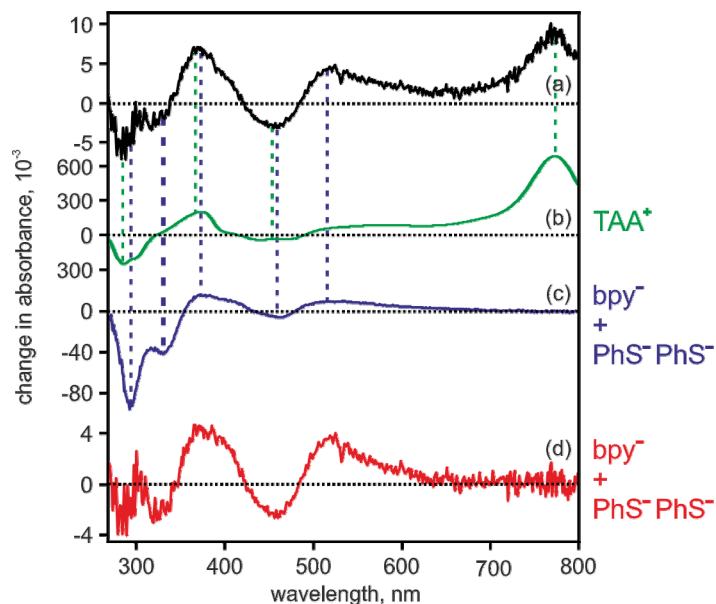


Figure S8. (a) Transient absorption spectrum of 5.0 μM heptad in dry de-aerated CH_3CN measured in a time window of 100 ns immediately following excitation at 532 nm with laser pulses of ca. 10 ns duration (same spectrum as in Figure 1a). (b) UV-Vis difference spectrum obtained after chemical oxidation of TAA to TAA^+ using $\text{Cu}(\text{ClO}_4)_2$ and the heptad (same spectrum as in Figure 1b). (c) UV-Vis difference spectrum obtained after electrochemical reduction of the heptad in CH_3CN containing 0.1 M TBAPF₆ at a potential of -1.8 V vs. SCE (same spectrum as in Figure S6b). (d) Spectrum obtained after subtracting the (appropriately scaled) green trace in (b) from the black trace in (a).

Yet another way to analyze the transient absorption and spectro-electrochemical data is presented in Figure S9. The black trace in Figure S9a is the transient absorption spectrum of the heptad from Figure 1a (identical to that in Figure S8a). The green trace in Figure S9a is the UV-Vis difference spectrum obtained after chemical oxidation of TAA to TAA^+ (same spectrum as in Figure 1b / S8b), but scaled to match the change in absorbance at 775 nm in the black spectrum). Subtraction of this green spectrum from the black spectrum in Figure S9a yields the difference spectrum shown as a red trace in Figure S9b. In this red spectrum the spectral contributions of all reduction products to the observable photoproduct have now been isolated. Further included in Figure S9b (as an orange trace) is the experimental UV-Vis difference spectrum from Figure S6a obtained after electrochemical reduction of the TAA-Ru reference complex, and this orange spectrum was scaled such that its change in absorbance at 520 nm matches the change in the red spectrum at that wavelength. When subtracting this orange spectrum from the red spectrum, it should be possible to isolate the spectral contribution of the PhSSPh reduction product. The result of this subtraction is shown as a dark blue trace in Figure S9c, and indeed the resulting derived spectrum is in very good agreement with the UV-Vis difference spectrum obtained after electrochemical reduction of the free $\text{bpy-xy-PhSSPh-xy-bpy}$ ligand at -2.0 V vs. SCE (light blue trace in Figure S9c, reproduced from Figure S5). This confirms that the key reduction product in the transient absorption spectrum is indeed the two-electron reduced form of PhSSPh.

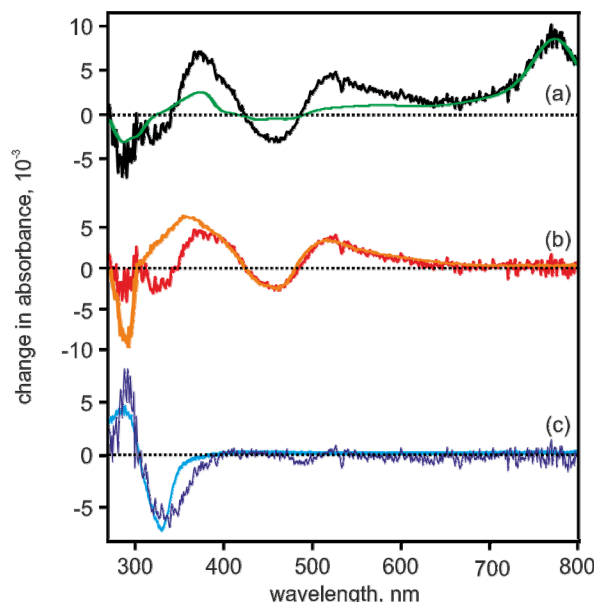


Figure S9. (a) Black trace: Transient absorption spectrum of 5.0 μM heptad in dry de-aerated CH_3CN , measured in a time window of 100 ns immediately following excitation at 532 nm with laser pulses of ca. 10 ns duration (same spectrum as in Figure 1a and in Figure S8a). Green trace: UV-Vis difference spectrum obtained after chemical oxidation of TAA to TAA^+ using $\text{Cu}(\text{ClO}_4)_2$ and heptad (reproduced from Figure S8b, scaled to match the change in absorbance at 775 nm in the black spectrum). (b) Red trace: Spectrum obtained after subtraction of the green trace from the black trace in (a). Orange trace: UV-Vis difference spectrum obtained after electrochemical reduction of the TAA-Ru reference complex (Scheme 1c) in CH_3CN containing 0.1 M TBAPF_6 at a potential of -1.6 V vs. SCE (reproduced from Figure S6a, scaled to match the change in absorbance at 520 nm in the red spectrum). (c) Dark blue trace: Spectrum obtained after subtraction of the orange trace from the red trace. Light blue trace: UV-Vis difference spectrum obtained after electrochemical reduction of the free bpy-xy-PhSSPh-xy-bpy ligand in CH_2Cl_2 with 0.1 M TBAPF_6 at a potential of -2.0 V vs. SCE (reproduced from in Figure S5, scaled to match the change in absorbance at 320 nm in the dark blue spectrum).

The transient absorption signal at 775 nm for the heptad in de-aerated CH_3CN at 22 $^\circ\text{C}$ decays in a tri-exponential manner (Figure S10). A fit to this data set yields the time constants with relative weighting factors reported in the main paper (summarized also in Table S2). Transients at 320 nm could not be measured due to the weakness of the signal in that spectral range (see beginning of this section for a brief discussion of sensitivity-related experimental challenges). Detection at 518 nm monitors predominantly the reduced photosensitizer unit ($\text{Ru}(\text{bpy})_3^+$), but there is also a small contribution of TAA^+ to the absorption at this wavelength. Thus, one observes primarily the $\text{TAA}^+ / \text{Ru}(\text{bpy})_3^+$ photoproduct pairs at this wavelength, and there is only a small contribution from the 2 $\text{TAA}^+ / \text{PhS}^+\text{PhS}^-$ key photoproduct (Figure S11). This manifests in the determination of essentially the same time constants but with different relative proportions when compared to the transient recorded at 775 nm (Table S2).

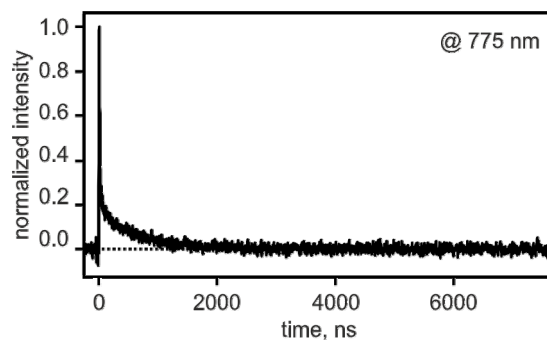


Figure S10. Normalized transient absorption decay of the heptad (5 μ M) at 775 nm in dry, de-aerated CH₃CN at 22 °C.

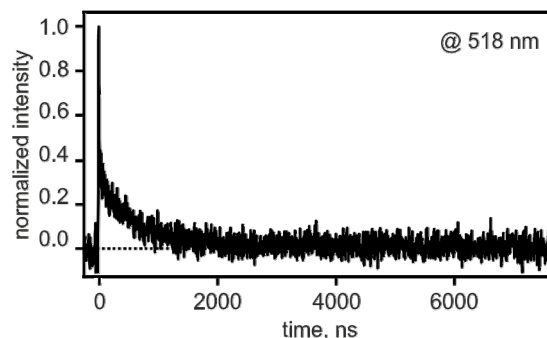


Figure S11. Normalized transient absorption decay of the heptad (5 μ M) at 518 nm in dry, de-aerated CH₃CN at 22 °C.

Table S2. Time constants and relative contributions of the different photoproducts observed for the heptad in de-aerated CH₃CN at different detection wavelengths (λ_{det}) following excitation at 532 nm with laser pulses of ca. 10 ns duration.

no.	photoproduct	$\lambda_{\text{det}} = 775 \text{ nm}$	$\lambda_{\text{det}} = 518 \text{ nm}$
I	TAA⁺-Ru(bpy)₃⁺-PhSSPh-Ru(bpy)₃²⁺-TAA	$\leq 10 \text{ ns}$ (80%)	$\leq 10 \text{ ns}$ (68%)
II	TAA⁺-Ru(bpy)₃²⁺-PhSSPh-Ru(bpy)₃⁺-TAA	645 ns (15%)	631 ns (28%)
III	TAA⁺-Ru(bpy)₃²⁺-PhS[•]PhS[•]-Ru(bpy)₃²⁺-TAA⁺	66 ns (5%)	67 ns (4%)

Photoproduct I forms simply via reductive ³MLCT excited state quenching by TAA. In closely related donor-sensitizer-acceptor compounds in which the donor-sensitizer distance was similar, this quenching step occurred with time constants around 10-65 ps.^{16b, 19} We investigated a range of related compounds in which the TAA⁺ / Ru(bpy)₃⁺ photoproduct pairs were formed by intramolecular electron transfer within less than 10 ns.^{14, 20}

Three different pathways for the formation of photoproduct II are conceivable. The simplest explanation would be intramolecular thermal through-bond electron transfer from Ru(bpy)₃⁺ to Ru(bpy)₃²⁺ in photoproduct I. Alternatively, for certain favorable geometrical arrangements of donor branches within a given heptad, there could be through-space hole transfer from TAA⁺ to TAA in photoproduct I. Such a pathway could be very important in some of the isomers of the molecular heptad. The third pathway involves further excitation of photoproduct I at the second Ru(bpy)₃²⁺ unit, followed by intramolecular through-bond electron transfer from Ru(bpy)₃⁺ to ³MLCT-excited Ru(bpy)₃²⁺. No attempts

were made to clarify which one of these pathways predominates, as the details regarding the formation of the side product II are beyond the scope of this study.

As noted in the main paper, photoproduct III is likely to form only from heptad molecules in which two TAA⁺ / Ru(bpy)₃³⁺ pairs are formed, because a hypothetical intermediate comprised of TAA⁺, Ru(bpy)₃²⁺, and disulfide monoanion (PhSSPh⁻) seems energetically inaccessible (Scheme S2). In other words, the PhSSPh moiety must be flanked by two Ru(bpy)₃³⁺ units in order for two-electron reduction to occur.

In order to determine which decay component (66 ns vs. 645 ns, Table S2) belongs to what photoproduct (II or III), transient absorption experiments with a time delay of 500 ns were performed (Figure S12).

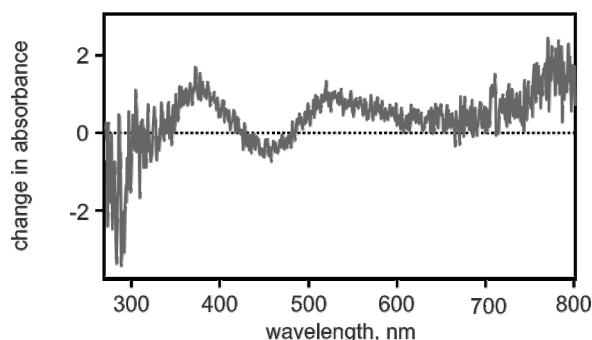


Figure S12. Transient absorption spectrum of 5.0 μM heptad in dry de-aerated CH_3CN at 22 $^\circ\text{C}$ measured in a time window of 100 ns, starting 500 ns after excitation at 532 nm with laser pulses of ca. 10 ns duration.

The bleach at 320 nm is no longer observable after 500 ns, indicating that the 66-ns time constant is caused by photoproduct III, as indicated in Table S2.

Determination of the quantum yield

The quantum yield for the formation of the desired two-electron reduction product was estimated by comparing the concentration of the ³MLCT-excited molecules of a solution Ru(bpy)₃²⁺ and the concentration of the desired photoproduct III formed upon laser excitation of the heptad. Excitation occurred at 532 nm and a pulse energy of ~34 mJ in both cases. A beam expander ensured that essentially the entire cuvette was irradiated with the pump laser.

A 5.5 μM solution of the heptad in neat CH₃CN (η = 1.34) was prepared and the absorbance at 532 nm measured (A_{532, heptad} = 0.03115). As a reference,²¹ two Ru(bpy)₃²⁺ solutions in H₂O (η = 1.33) with concentrations of (i) 3.2 and (ii) 4.7 μM were prepared. A_{532, ref} of both samples are summarized in Table S3. Since A₅₃₂ of the heptad and A_{532, ref} of the Ru(bpy)₃²⁺ reference solutions are not the same, a correction factor (f_n) is applied (see equation S1 and Table S3).

$$f_n = A_{532, \text{heptad}} / A_{532, \text{ref}} \quad (\text{eq. S1})$$

To estimate the concentration of the ³MLCT-excited Ru(bpy)₃²⁺ molecules (c_{ref}), the difference in absorbance at 455 nm (ΔA₄₅₅) upon excitation at 532 nm was measured (see Table S3). On the basis of the Lambert–Beer law and taking the correction factor f_n into account, an average concentration c_{ref, Ø} = 7.66 μM was determined using ε₄₅₅ = 10100 L mol⁻¹ cm⁻¹ and equation S2.²²

$$\Delta A_{455} \cdot f_n = \epsilon_{455} \cdot c \cdot d \quad (\text{eq. S2})$$

Table S3. Key parameters relevant for the determination of the concentration of ³MLCT-excited Ru(bpy)₃²⁺.

Ru(bpy) ₃ ²⁺	(i)	(ii)
A _{532, ref}	0.02273	0.03410
f _n	1.371	0.914
ΔA ₄₅₅	0.05712	0.08369
c _{ref, Ø}	7.75 μM	7.57 μM

To determine the concentration of the desired twofold charge-separated product in the molecular heptad, the decay in absorbance of the TAA band at 775 nm was measured. A tri-exponential fit gave an absorbance of A_{775, III} = 0.00234 for the key photoproduct III. Since this product consists of two oxidized TAA groups, A_{775, III} needs to be divided by a factor of 2 prior to the estimation of the concentration with the Lambert-Beer law. Using the known extinction coefficient of one TAA moiety at 775 nm (ε₇₇₅ = 32000 L mol⁻¹ cm⁻¹) a concentration of c_{heptad, III} = 3.65·10⁻⁸ M was estimated.²³

The quantum yield for the formation of the desired two-electron reduction product (ϕ_{III}) was estimated based on equation S3.

$$\phi_{\text{III}} = C_{\text{heptad, III}} / C_{\text{ref, } \emptyset} \quad (\text{eq. S3})$$

Table S4. Changes in absorbance at 775 nm, concentrations, and quantum yields (ϕ_n) for the individual photoproducts (n = I, II, III) formed in the molecular heptad.

	photoproduct I	photoproduct II	photoproduct III
ΔA_{775}^a	0.01876	0.00338	0.00234 / 2
C _{heptad, n}	$5.86 \cdot 10^{-7} \text{ M}$	$1.06 \cdot 10^{-7} \text{ M}$	$3.65 \cdot 10^{-8} \text{ M}$
ϕ_n	7.7%	1.4%	0.5%

^a Determined from tri-exponential fits to experimental decay curves recorded at 775 nm as described in the text.

The analysis in the main paper shows that under acidic conditions the resulting key photoproduct is comprised of two TAA^+ units and one PhSSPh moiety which has been reduced to PhSHPhSH . In addition to this desired two-electron photoproduct, contributions from other excited states of the heptad are expected, in particular from the $\text{TAA}^+ - \text{Ru}(\text{bpy})_3^{2+} - \text{PhSSPh} - \text{Ru}(\text{bpy})_3^+ - \text{TAA}$ side product also observed in neat CH_3CN , and from the very short-lived $\text{TAA}^+ - \text{Ru}(\text{bpy})_3^+ - \text{PhSSPh} - \text{Ru}(\text{bpy})_3^{2+} - \text{TAA}$ primary product. The twofold charge-separated state containing PhSHPhSH is the only photoproduct that is expected to be strongly influenced by the presence of acid, due to the expected protonation of the dithiolate reduction product. By contrast, for the $\text{TAA}^+ - \text{Ru}(\text{bpy})_3^{2+} - \text{PhSSPh} - \text{Ru}(\text{bpy})_3^+ - \text{TAA}$ and $\text{TAA}^+ - \text{Ru}(\text{bpy})_3^+ - \text{PhSSPh} - \text{Ru}(\text{bpy})_3^{2+} - \text{TAA}$ states similar decay times as for neat CH_3CN solution are anticipated. In the presence of 0.1 M monochloroacetic acid, the transient absorption signal at 775 nm decays much more slowly than in neat CH_3CN (blue trace in Figure S13, compared to black trace in Figure S10).

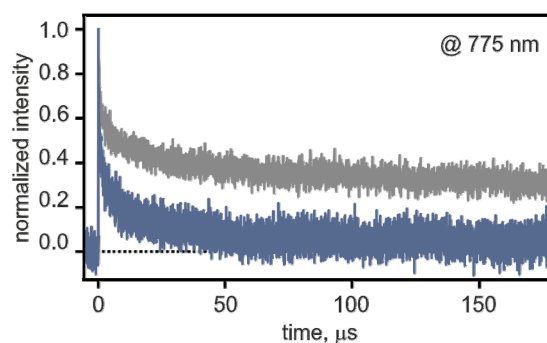


Figure S13. Grey trace: Transient absorption decay of the heptad (5 μM) at 775 nm in dry, de-aerated CH_3CN with 0.1 M TsOH at 22 $^\circ\text{C}$. Blue trace: Transient absorption decay of the heptad (5 μM) at 775 nm in dry, de-aerated CH_3CN with 0.1 M monochloroacetic acid at 22 $^\circ\text{C}$.

Monochloroacetic acid has a pK_a value of 18.8 in CH_3CN ,²⁴ and *p*-toluenesulfonic acid (TsOH) is substantially stronger with a pK_a of 8.6 in the same solvent.²⁵ In the presence of 0.1 M TsOH , the contribution from very slowly decaying photoproducts is further increased (grey trace in Figure S13), and even beyond 150 μs the transient absorption signal at 775 nm has not decayed back to baseline. On this timescale bimolecular reactions are expected to occur and exponential fits to the experimental data are no longer meaningful. The exceedingly slow decay observed in this experiment forms the basis for the possibility of forming the dithiol photoproduct under steady-state LED irradiation (Figure 2 of the main paper). Possible reasons for the longevity of the dithiol photoproduct are discussed in the next section.

According to the energy-level scheme in Scheme S2, the **TAA⁺-Ru(bpy)₃²⁺-PhS[•]PhS[•]-Ru(bpy)₃²⁺-TAA⁺** key photoproduct (no. III in Table S2 and Figure S13) is ca. 3.3 eV above the electronic ground state in neat CH₃CN. The dithiolate product is expected to be protonated by TsOH. The reaction free energy (ΔG_{PT}^0) for protonation of PhS[•]PhS[•] by TsOH can be estimated on the basis of equation S4.

$$\Delta G_{PT}^0 = -e \cdot 0.059 \text{ V} \cdot pK_a(\text{PhSHPhS}) - pK_a(\text{TsOH}) \quad (\text{eq. S4})$$

The acidity constant (pK_a) of TsOH in CH₃CN is 8.6.²⁵ For PhSHPhSH the pK_a in CH₃CN is not known. As an approximation, the pK_a value of thiophenol in DMSO (10.3)²⁶ was converted into the pK_a in CH₃CN using a known expression (equation S5).²⁵ Thus, a pK_a value of 22.4 was estimated for the two thiophenol moieties of PhSHPhSH in CH₃CN.

$$pK_a(\text{in CH}_3\text{CN}) = 12.31 + 0.98 \cdot pK_a(\text{in DMSO}) \quad (\text{eq. S5})$$

Evidently, TsOH is a much stronger acid than PhSHPhSH in CH₃CN. For ΔG_{PT}^0 one therefore obtains a value of -0.8 eV, representing the driving-force for a single protonation step. Consequently, for twofold protonation of PhS[•]PhS[•] by two equivalents of TsOH, a driving-force of -1.6 eV is estimated. This implies that the final **TAA⁺-Ru(bpy)₃²⁺-PhSHPhSH-Ru(bpy)₃²⁺-TAA⁺** photoproduct formed in presence of TsOH should be stabilized by 1.6 eV relative to its unprotonated **TAA⁺-Ru(bpy)₃²⁺-PhS[•]PhS[•]-Ru(bpy)₃²⁺-TAA⁺** counterpart formed in neat CH₃CN (photoproduct III in Table S2 and Scheme S2), leading to an energy of 3.3 eV - 1.6 eV = 1.7 eV for **TAA⁺-Ru(bpy)₃²⁺-PhSHPhSH-Ru(bpy)₃²⁺-TAA⁺**.

However, the observed stability of the **TAA⁺-Ru(bpy)₃²⁺-PhSHPhSH-Ru(bpy)₃²⁺-TAA⁺** photoproduct (Figure 2a in the main paper) suggests that this photoproduct is actually more stable than the initial **TAA-Ru(bpy)₃²⁺-PhSSPh-Ru(bpy)₃²⁺-TAA** ground state, and this in turn implies that the pK_a of thiophenol is a poor approximation for the actual pK_a value of the two SH groups in our central acceptor. Thus, it is difficult to obtain a reliable estimate for the driving-force of the proton-coupled electron transfer (PCET) reaction between two TsOH molecules and PhSSPh in CH₃CN.

Thiol-disulfide interchange is a fundamental process to reduce disulfides and to oxidize thiols.²⁷ This reaction commonly occurs via an S_N2 mechanism.²⁸ The thiolate nucleophile attacks the disulfide from the backside, forming a trisulfide-like transition state.²⁷ A common reducing agent for enzyme activation is dithiothreitol (DTT^{red}).²⁹ Usually added in excess amounts, it reduces the disulfides via two sequential thiol-disulfide exchange reactions. The twofold charge-separated state of the heptad (no. III in Table S2) also contains two thiolate groups, thus a sequential thiolate-disulfide interchange reaction should also be possible. The advantage of the heptad compared to DTT^{red} or other common reducing agents is that the exchange can be performed catalytically. The proposed mechanism with the heptad as the catalyst is shown in Scheme 2a of the main paper.

At first, formation of the twofold charge-separated state of the heptad is induced by visible light, followed by reduction of the oxidized TAA groups by a sacrificial electron donor. Two subsequent thiol-disulfide exchange reactions with another disulfide can then occur, reducing it to a dithiolate and oxidizing the catalyst to the initial disulfide, i. e., the ground state, which closes the catalytic cycle.

Disulfides are known to have large one-electron reduction potentials. A few experimentally determined potentials of aliphatic acyclic and cyclic disulfides can be found in the literature, ranging from -2.72 V vs. SCE for di-*tert*.-butyl disulfide to -1.65 V vs. SCE for diphenyl disulfide (both in DMF).³⁰ 1,2-Ditholane is reduced at -1.77 V vs. SCE in CH₃CN.³¹ On the basis of thermodynamic considerations, Ru(bpy)₃²⁺-like complexes in their reduced form ($E^0 = -1.3$ V vs. SCE in CH₃CN, Table S1) should not be able to reduce such disulfides via two subsequent single electron transfers (SETs). However, it was shown that it is possible to reduce disulfides using reductants with less negative reduction potentials, for example for the reduction of acyclic aliphatic and aromatic disulfides.^{30, 32} Specifically, electrochemically generated radical anions of several molecules were used as electron donors, and even though many of them had significantly less negative reduction potentials compared to those of the disulfides, the latter were reduced in all cases. It was found that the disulfides dissociate after SET via a so-called “loose radical-ion dissociative electron-transfer mechanism”.^{32a} In the course of electron uptake, the disulfide bond elongates and a loose radical anion is formed, in which the SOMO is localized at the disulfide bond, and the S-S bond can cleave (Scheme 2b in the main paper).^{32a} The formed thiyl radical can then be reduced in a second step.

Although disulfides can be reduced via SET, it may be more efficient via thiol-disulfide interchange. To counteract dissociative SET reduction, the *trans*-4,5-dihydroxy-1,2-dithiane (DTT^{ox}) substrate was used. Due to its cyclic structure, the disulfide bond cleavage upon SET reduction is entropically less favored compared to acyclic disulfides, such that it may stay intact, or not even be reduced with SET donors.

In the following, the results of the reduction of DTT^{ox} catalyzed by the heptad and by the Ru(bpy)₃²⁺ and TAA-Ru reference compounds are presented. Reactions were performed in de-aerated, deuterated solvent in flame-sealed NMR tubes under an Ar atmosphere and continuous LED irradiation (3.5 W) at 455 nm for 20 hours. Product formation was monitored by ¹H NMR spectroscopy (400 MHz or 600 MHz). Conversions were calculated by integrating one substrate peak and the corresponding product peak. The product yield was determined with an error of approximately

$\pm 0.2\%$. The turnover number (TON) was calculated by dividing the product concentration by the catalyst concentration. The sacrificial donor triethylamine (TEA) was present at 100 mM concentration and the substrate (DTT^{ox}) concentration was 22 mM. The concentration of heptad was 20 μM , while in the cases of the TAA-Ru and Ru(bpy)₃²⁺ reference compounds a concentration of 40 μM was employed to account for the fact that the heptad comprises two photosensitizer units. The key results are summarized in Table S5.

Table S5. Product yields and TONs of the reduction of DTT^{ox} catalyzed by the heptad or the Ru(bpy)₃²⁺ and TAA-Ru reference compounds (Scheme 1d) in dry, de-aerated CH₃CN in the presence of excess TEA as reductant.

entry	catalyst	sacrificial donor	h ν (455 nm)	yield / % ^a	TON ^a
1	TAA-Ru	TEA	✓	1.6	9
2	Ru(bpy) ₃ ²⁺	TEA	✓	1.5	9
3	heptad	TEA	✓	3.6	41
4	heptad	none	✓	0	0
5	heptad	TEA	✗	0	0
6	heptad	ascorbate	✓	0	0

^a Extracted from the ¹H NMR data in Figures S14-S17.

The significantly higher yield and TON observed with the heptad (entry 3) compared to the TAA-Ru or Ru(bpy)₃²⁺ reference compounds (entries 1 and 2) suggests that the heptad is indeed able to catalyze DTT^{ox} reduction by thiolate-disulfide interchange, as discussed in the main paper. The observation of non-zero yields and TONs for the reference compounds signals the reduction of DTT^{ox} via an SET reaction pathway. As noted in the main paper, the sacrificial donor TEA promotes this reaction path, because after its initial SET oxidation and subsequent deprotonation, the resulting α -amino alkyl radical is a very potent donor, far stronger than the initial TEA compound.³³ Thus, a single photoexcitation can trigger overall two-electron oxidation of TEA coupled to two-electron reduction of a substrate. Many of the currently known sacrificial donors suffer from this problem.³⁴ Sodium ascorbate was tested in a 1:4 mixture of CH₃CN and H₂O, but in this case no product accumulation occurs because ascorbate is a reversible electron donor.

The product yields reported in Table S3 are low, because the equilibrium of the reaction $\text{PhS}^-\text{PhS}^- + \text{DTT}^{\text{ox}} \rightleftharpoons \text{PhSSPh} + \text{DTT}^{\text{red}}$ strongly disfavors product formation as noted in the main paper and as explained in the following. The reaction free energy (ΔG_4) of the thiolate-disulfide interchange between the PhS^-PhS^- (reduced dibenzo[1,2]dithiin of the heptad catalyst) and DTT^{ox} can be estimated using a thermodynamic cycle based on bond dissociation energies (BDEs) and pK_a values (Scheme S3). Since the BDEs of dibenzo[1,2]dithiin and DTT^{ox} as well as the pK_a value of the PhSHPhSH unit are not known, the corresponding values of thiophenol ³⁵ and methanethiol ³⁶ were taken (Table S6).



Scheme S3. Thermodynamic cycle for the reaction of thiophenol and methanethiol, used to estimate the reaction free energy for thiolate disulfide-interchange between PhS^-PhS^- and DTT^{ox} .

Table S6. Gas-phase bond dissociation energies (BDEs) and acidity constants (pK_a) in CH_3CN .

compound / relevant bond	BDE / kcal/mol	pK_a ^a
PhS-SPh	55 ^b	
PhS-H	83 ^c	22.4 ^f
$\text{CH}_3\text{S-SCH}_3$	65 ^d	
$\text{CH}_3\text{S-H}$	87 ^e	
DTT^{red} (RS-SR)		25.9 ^f

^a Converted from values reported for DMSO solution to CH_3CN solution using equation S5. ^b From ref. ^{35a}; ^c from ref. ^{35b}; ^d from ref. ^{36a}; ^e from ref. ^{36b}; ^f from ref. ²⁶.

Assuming that entropic and solvation effects can be neglected, the reaction free energies $\Delta G_1 - \Delta G_4$ in Scheme S3 can be calculated as follows:

$$\begin{aligned}\Delta G_1 &= -2.303 \cdot R \cdot T \cdot \text{pK}_a(\text{PhSH}) = -2.303 \cdot 8.3145 \text{ J mol}^{-1} \text{ K}^{-1} \cdot 298 \text{ K} \cdot 22.4 = -128 \text{ kJ mol}^{-1} \\ &= -30.6 \text{ kcal mol}^{-1}\end{aligned}\quad (\text{eq. S6})$$

$$\begin{aligned}\Delta G_2 &= \Sigma \text{BDE}_{\text{broken}} - \Sigma \text{BDE}_{\text{formed}} = 2 \cdot 83 \text{ kcal mol}^{-1} + 65 \text{ kcal mol}^{-1} - 2 \cdot 87 \text{ kcal mol}^{-1} - 55 \text{ kcal mol}^{-1} \\ &= 2.0 \text{ kcal mol}^{-1}\end{aligned}\quad (\text{eq. S7})$$

$$\begin{aligned}\Delta G_3 &= -2.303 \cdot R \cdot T \cdot \text{pK}_a(\text{DTT}^{\text{red}}) = -2.303 \cdot 8.3145 \text{ J mol}^{-1} \text{ K}^{-1} \cdot 298 \text{ K} \cdot 25.9 = -148 \text{ kJ mol}^{-1} \\ &= -35.4 \text{ kcal mol}^{-1}\end{aligned}\quad (\text{eq. S8})$$

$$\begin{aligned}\Delta G_4 &= \Delta G_1 + \Delta G_2 \quad \Delta G_3 = -30.6 \text{ kcal mol}^{-1} + 2.0 \text{ kcal mol}^{-1} + 35.4 \text{ kcal mol}^{-1} \\ &= +6.8 \text{ kcal mol}^{-1}\end{aligned}\quad (\text{eq. S9})$$

This calculation shows that thiolate-disulfide interchange between the reduced benzo[1,2]dithiin unit of the heptad and DDT^{ox} is thermodynamically uphill, and this can account for the fact that only low overall DTT^{red} product yields can be achieved (Table S5). Although this is only a rough approximation, the positive value of ΔG_4 clearly indicates that the reaction equilibrium is strongly on the reactant side. For this reason, the conversion of DTT^{ox} to DTT^{red} by thiolate-disulfide interchange with the heptad cannot be significantly increased. By increasing the reaction time to 48 h or more, the yields only increase slightly, indicating that the equilibrium is almost reached.

The data in Table S5 were extracted from the ¹H NMR spectra shown in the following.

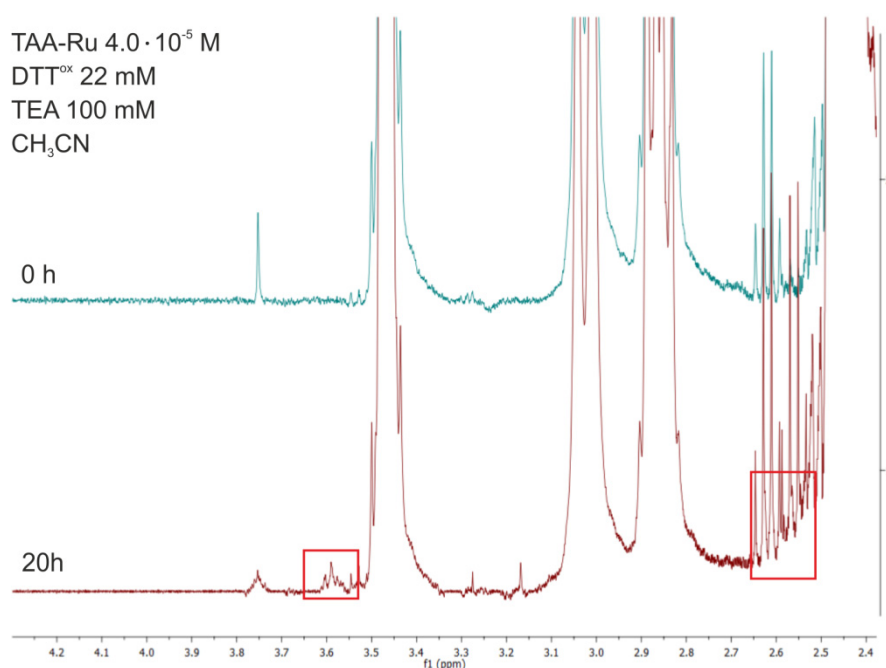


Figure S14. ¹H NMR spectra corresponding to entry 1 of Table S5.

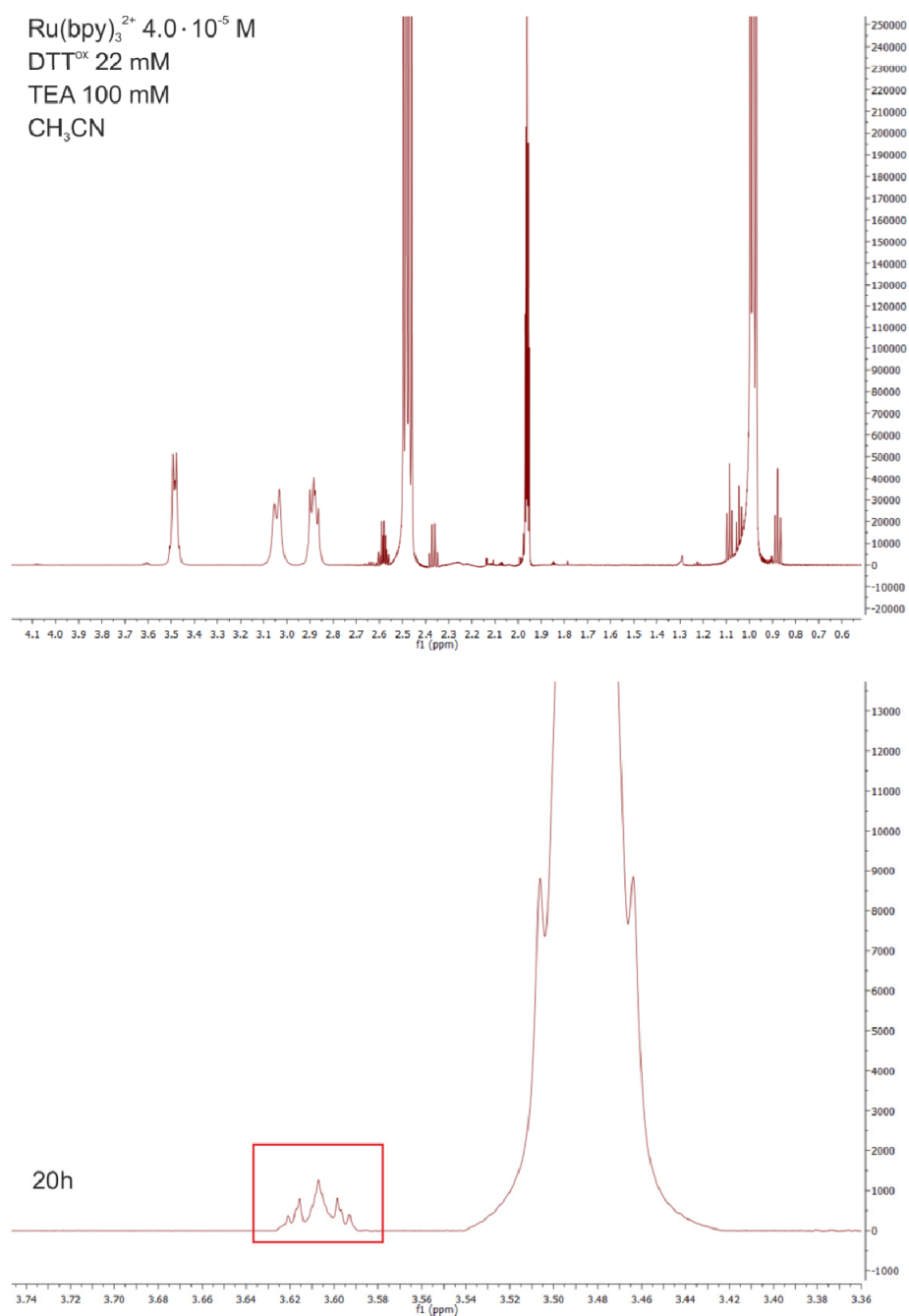


Figure S15. ^1H NMR spectra corresponding to entry 2 of Table S5.

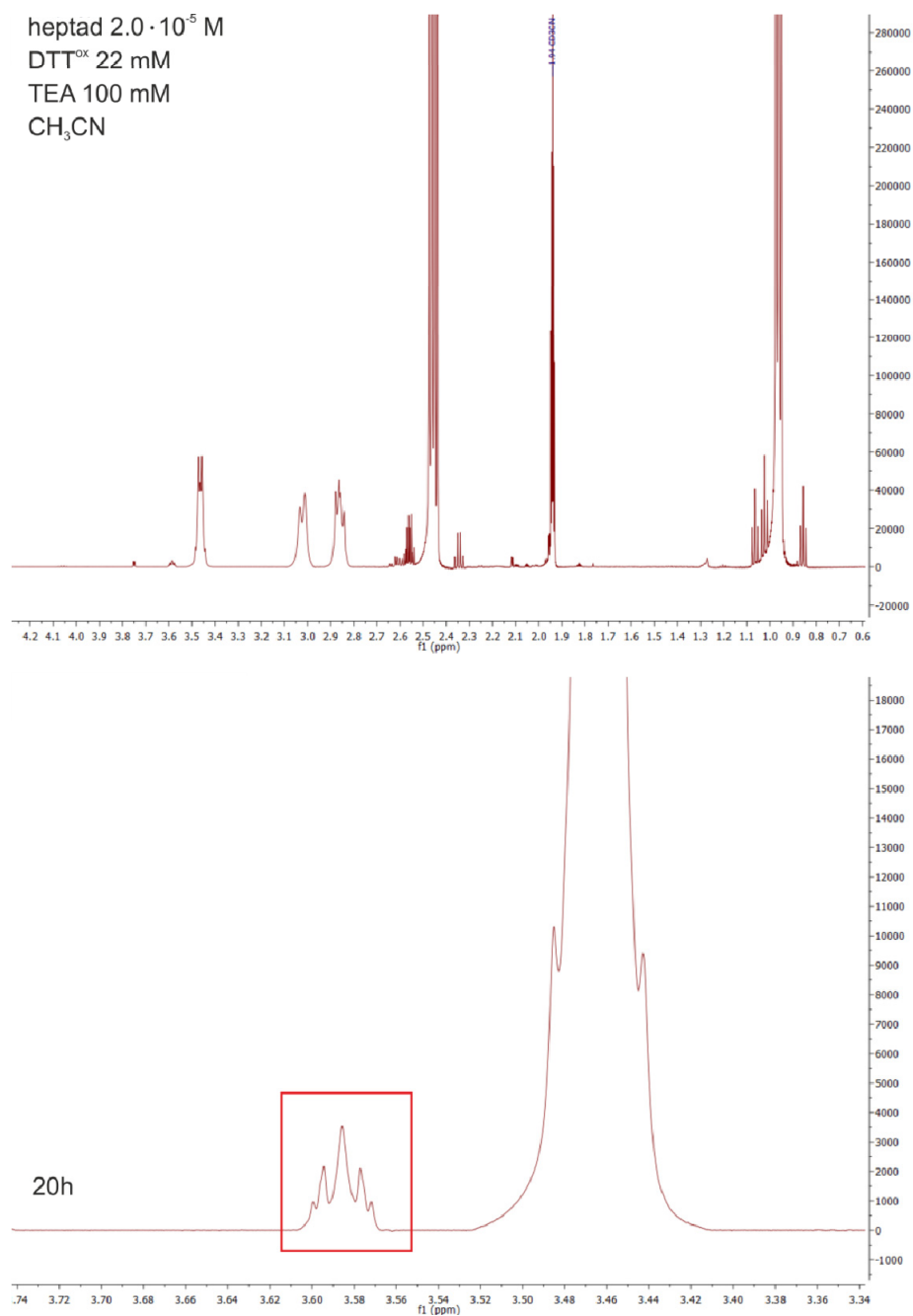


Figure S16. ^1H NMR spectra corresponding to entry 3 of Table S5.

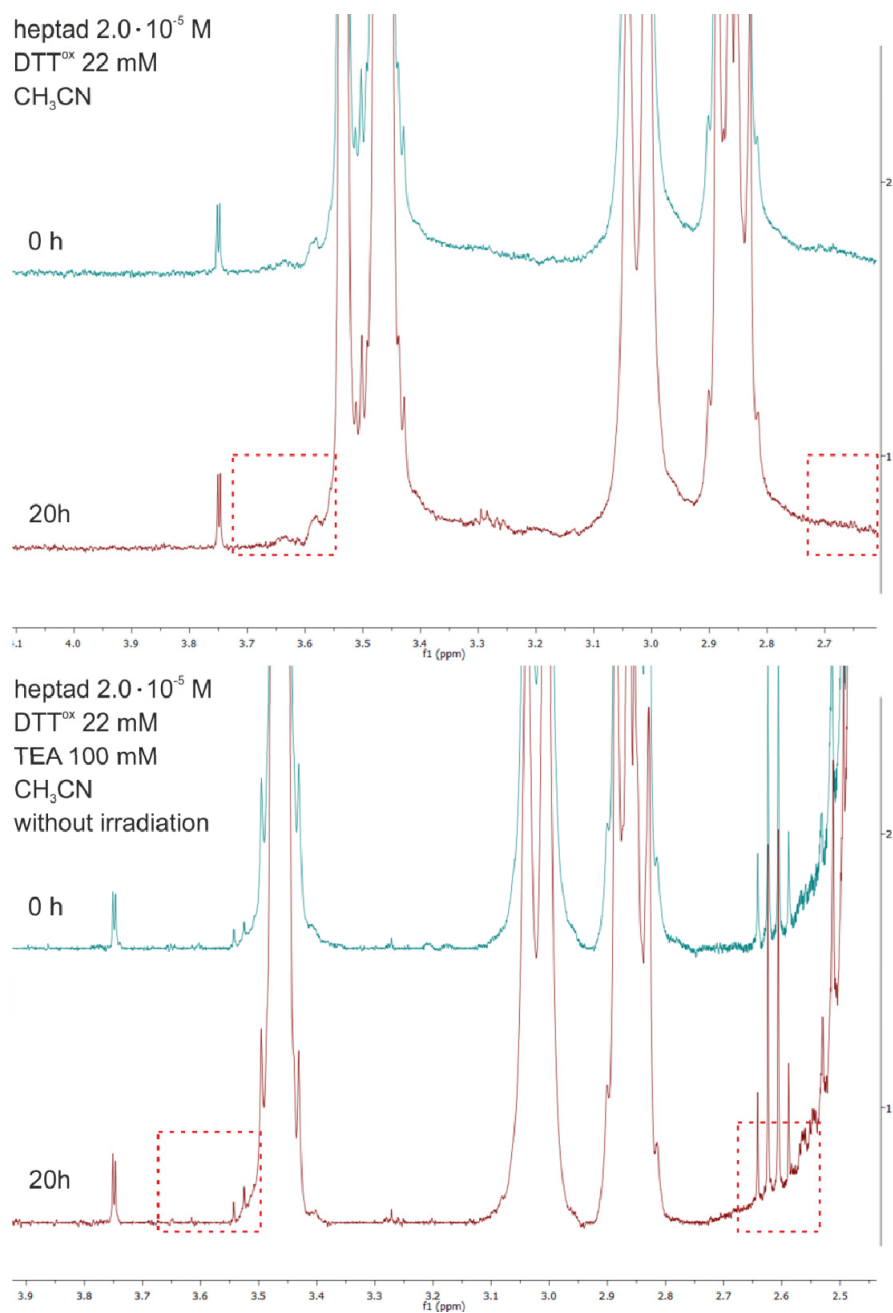
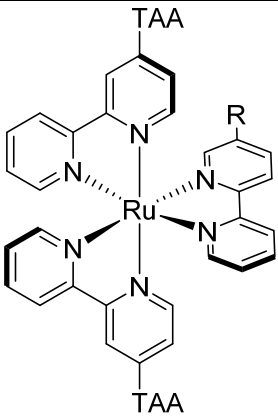
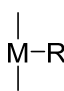
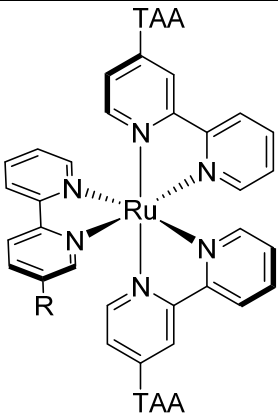
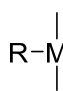
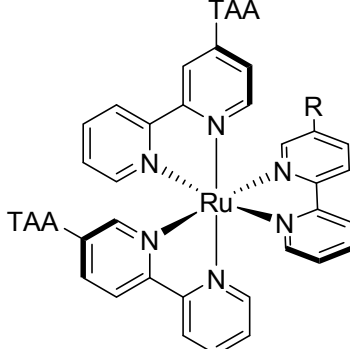
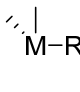
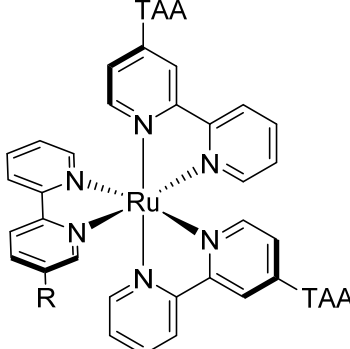
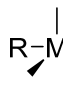
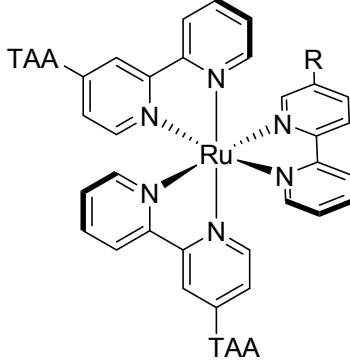
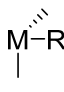
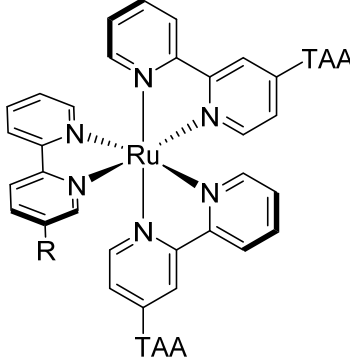



Figure S17. ¹H NMR spectra corresponding to entries 4 and 5 of Table S5.

Isomers and shortest TAA-TAA distances

As mentioned in the main paper, the design of the heptad, in which mono-triarylamine (TAA) substituted bipyridine ligands are utilized, results in the formation of several stereoisomers. This primarily arises due to the non-inequivalent nature of equatorial and axial positions around an octahedral Ru center with respect to the main ligand and the chirality of the Ru center, resulting in 8 stereoisomers per Ru center (Table S6). As the heptad contains two Ru centers, one can envisage 64 possible combinations, 40 of which are unique stereoisomers (Table S7).

Table S6. Chemical structure and notation of all possible stereoisomers at each chiral center.

Λ		Δ	
structure	notation	structure	notation
			
			
			

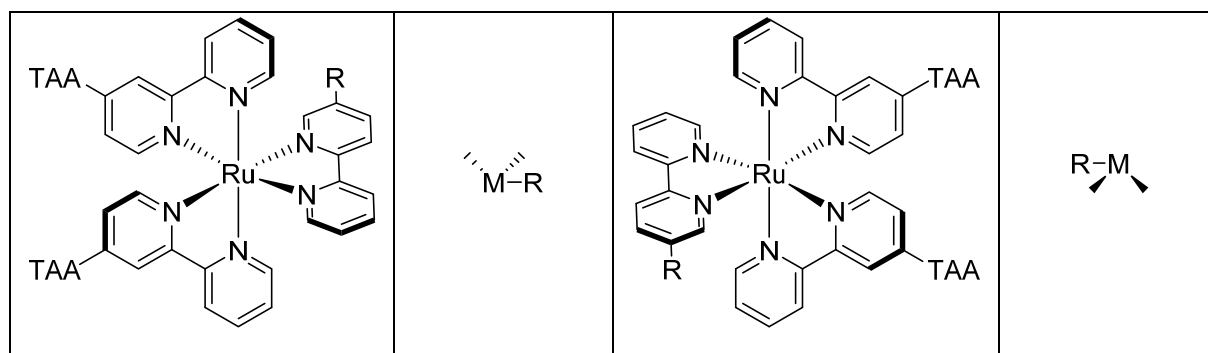
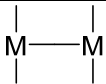
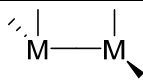
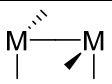
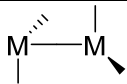
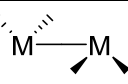
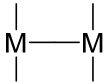
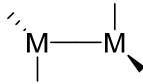
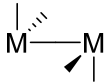
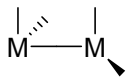
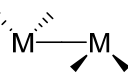


Table S7. Notations for all possible stereoisomers of the heptad.

$\Lambda - \Lambda$	$\Lambda - \Delta$
<p>Diagram showing the first row of stereoisomers for the $\Lambda - \Lambda$ case. It consists of two metal-metal bonds, each represented by a horizontal line with vertical bonds at the ends.</p>	<p>Diagram showing the first row of stereoisomers for the $\Lambda - \Delta$ case. It consists of two metal-metal bonds, each represented by a horizontal line with vertical bonds at the ends.</p>
<p>Diagram showing the second row of stereoisomers for the $\Lambda - \Lambda$ case. It consists of two metal-metal bonds, each represented by a horizontal line with vertical bonds at the ends.</p>	<p>Diagram showing the second row of stereoisomers for the $\Lambda - \Delta$ case. It consists of two metal-metal bonds, each represented by a horizontal line with vertical bonds at the ends.</p>
<p>Diagram showing the third row of stereoisomers for the $\Lambda - \Lambda$ case. It consists of two metal-metal bonds, each represented by a horizontal line with vertical bonds at the ends.</p>	<p>Diagram showing the third row of stereoisomers for the $\Lambda - \Delta$ case. It consists of two metal-metal bonds, each represented by a horizontal line with vertical bonds at the ends.</p>
<p>Diagram showing the fourth row of stereoisomers for the $\Lambda - \Lambda$ case. It consists of two metal-metal bonds, each represented by a horizontal line with vertical bonds at the ends.</p>	<p>Diagram showing the fourth row of stereoisomers for the $\Lambda - \Delta$ case. It consists of two metal-metal bonds, each represented by a horizontal line with vertical bonds at the ends.</p>
$\Delta - \Lambda$	$\Delta - \Delta$
<p>Diagram showing the first row of stereoisomers for the $\Delta - \Lambda$ case. It consists of two metal-metal bonds, each represented by a horizontal line with vertical bonds at the ends.</p>	<p>Diagram showing the first row of stereoisomers for the $\Delta - \Delta$ case. It consists of two metal-metal bonds, each represented by a horizontal line with vertical bonds at the ends.</p>
<p>Diagram showing the second row of stereoisomers for the $\Delta - \Lambda$ case. It consists of two metal-metal bonds, each represented by a horizontal line with vertical bonds at the ends.</p>	<p>Diagram showing the second row of stereoisomers for the $\Delta - \Delta$ case. It consists of two metal-metal bonds, each represented by a horizontal line with vertical bonds at the ends.</p>
<p>Diagram showing the third row of stereoisomers for the $\Delta - \Lambda$ case. It consists of two metal-metal bonds, each represented by a horizontal line with vertical bonds at the ends.</p>	<p>Diagram showing the third row of stereoisomers for the $\Delta - \Delta$ case. It consists of two metal-metal bonds, each represented by a horizontal line with vertical bonds at the ends.</p>
<p>Diagram showing the fourth row of stereoisomers for the $\Delta - \Lambda$ case. It consists of two metal-metal bonds, each represented by a horizontal line with vertical bonds at the ends.</p>	<p>Diagram showing the fourth row of stereoisomers for the $\Delta - \Delta$ case. It consists of two metal-metal bonds, each represented by a horizontal line with vertical bonds at the ends.</p>

One consequence of the various diastereoisomers is that the heptad can exist in a range of conformations in which the TAA donors can approach the central PhSSPh acceptor and one another (Table S8). As such, it is not surprising that the formed radical cation may migrate between TAA donors (across both Ru centers) in certain stereoisomers, resulting in the 645-ns decay component. Furthermore, as some stereoisomers can have the TAA donors approach the PhSSPh acceptor, it is not unreasonable to expect rapid decay of the charge-accumulated state.

Table S8. Shortest distances between TAA N-atoms (in Å) for representative stereoisomers, obtained from MMFF geometry optimization calculations.

$\Lambda - \Lambda$					
					
Ru ₁ -Ru ₂	25.5	25.5	25.3	24.9	25.3
TAA ₁ (Ax)-TAA ₁ (Ax)	21.2	-	-	-	-
TAA ₁ (Ax)-TAA ₁ (Eq)	-	16.4	16.5	16.5	-
TAA ₁ (Eq)-TAA ₁ (Eq)	-	-	-	-	16.3
TAA ₁ (Ax)-TAA ₂ (Ax)	19.5	19.7	33.5	40.3	-
TAA ₁ (Ax)-TAA ₂ (Eq)	-	31.5	25.0	13.4	-
TAA ₁ (Eq)-TAA ₂ (Eq)	-	43.6	13.0	26.0	12.8
$\Delta - \Lambda$					
					
Ru ₁ -Ru ₂	25.5	25.5	24.2	23.1	25.0
TAA ₁ (Ax)-TAA ₁ (Ax)	21.2	-	-	-	-
TAA ₁ (Ax)-TAA ₁ (Eq)	-	16.5	16.4	16.1	-
TAA ₁ (Eq)-TAA ₁ (Eq)	-	-	-	-	15.8
TAA ₁ (Ax)-TAA ₂ (Ax)	23.6	28.3	36.3	22.1	-
TAA ₁ (Ax)-TAA ₂ (Eq)	-	30.5	20.4	6.8	-
TAA ₁ (Eq)-	-	42.9	13.5	20.5	10.5

TAA ₂ (Eq)					
-----------------------	--	--	--	--	--

Molecular mechanics energy minimization calculations were performed at the Merck Molecular Force Field (MMFF) level of theory using Spartan '08 Version 1.2.0. To avoid local minima, bond angles of optimized structures were manually altered and re-optimized until a global minimum was found.

References

- (1) Gottlieb, H. E.; Kotlyar, V.; Nudelman, A., *J. Org. Chem.* **1997**, *62*, 7512-7515.
- (2) Bandarage, U. K.; Simpson, J.; Smith, R. A. J.; Weavers, R. T., *Tetrahedron* **1994**, *50*, 3463-3472.
- (3) Benniston, A. C.; Hagon, J.; He, X. Y.; Yang, S. J.; Harrington, R. W., *Org. Lett.* **2012**, *14*, 506-509.
- (4) Delogu, G.; Fabbri, D.; Dettori, M. A., *Tetrahedron: Asymmetry* **1998**, *9*, 2819-2826.
- (5) Wang, D. H.; Shen, Z. H.; Guo, M. M.; Cheng, S. Z. D.; Harris, F. W., *Macromolecules* **2007**, *40*, 889-900.
- (6) Yadav, G. D.; Lande, S. V., *Adv. Synth. Catal.* **2005**, *347*, 1235-1241.
- (7) Keyworth, C. W.; Chan, K. L.; Labram, J. G.; Anthopoulos, T. D.; Watkins, S. E.; McKiernan, M.; White, A. J. P.; Holmes, A. B.; Williams, C. K., *J. Mater. Chem.* **2011**, *21*, 11800-11814.
- (8) Cho, Y. H.; Kina, A.; Shimada, T.; Hayashi, T., *J. Org. Chem.* **2004**, *69*, 3811-3823.
- (9) Benniston, A. C.; Allen, B. D.; Harriman, A.; Llarena, I.; Rostron, J. P.; Stewart, B., *New J. Chem.* **2009**, *33*, 417-427.
- (10) Kuss-Petermann, M.; Wenger, O. S., *J. Phys. Chem. A* **2013**, *117*, 5726-5733.
- (11) Hankache, J.; Wenger, O. S., *Chem. Commun.* **2011**, *47*, 10145-10147.
- (12) Chen, J.; Kuss-Petermann, M.; Wenger, O. S., *Chem. Eur. J.* **2014**, *20*, 4098-4104.
- (13) Kuss-Petermann, M.; Wolf, H.; Stalke, D.; Wenger, O. S., *J. Am. Chem. Soc.* **2012**, *134*, 12844-12854.
- (14) Kuss-Petermann, M.; Wenger, O. S., *Angew. Chem. Int. Ed.* **2016**, *55*, 815-819.
- (15) Hall, G. B.; Kottani, R.; Felton, G. A. N.; Yamamoto, T.; Evans, D. H.; Glass, R. S.; Lichtenberger, D. L., *J. Am. Chem. Soc.* **2014**, *136*, 4012-4018.
- (16) (a) Roundhill, D. M., *Photochemistry and Photophysics of Metal Complexes*. Plenum Press: New York, 1994.
(b) Hankache, J.; Niemi, M.; Lemmetyinen, H.; Wenger, O. S., *Inorg. Chem.* **2012**, *51*, 6333-6344. (c) Lambert, C.; Nöll, G., *J. Am. Chem. Soc.* **1999**, *121*, 8434-8442.
- (17) (a) Braterman, P. S.; Song, J. I., *J. Org. Chem.* **1991**, *56*, 4678-4682. (b) Carlson, C. N.; Kuehl, C. J.; Ogallo, L.; Shultz, D. A.; Thompson, J. D.; Kirk, M. L.; Martin, R. L.; John, K. D.; Morris, D. E., *Organometallics* **2007**, *26*, 4234-4242.
- (18) Heath, G. A.; Yellowlees, L. J.; Braterman, P. S., *J. Chem. Soc., Chem. Commun.* **1981**, 287-289.
- (19) Oraziatti, M.; Kuss-Petermann, M.; Hamm, P.; Wenger, O. S., *Angew. Chem. Int. Ed.* **2016**, *55*, 9407-9410.
- (20) Kuss-Petermann, M.; Wenger, O. S., *J. Am. Chem. Soc.* **2016**, *138*, 1349-1358.
- (21) Müller, P.; Brettel, K., *Photochem. Photobiol. Sci.* **2012**, *11*, 632-636.
- (22) Goetz, M.; Kerzig, C.; Naumann, R., *Angew. Chem. Int. Ed.* **2014**, *53*, 9914-9916.
- (23) Sreenath, K.; Thomas, T. G.; Gopidas, K. R., *Org. Lett.* **2011**, *13*, 1134-1137.
- (24) Muckerman, J. T.; Skone, J. H.; Ning, M.; Wasada-Tsutsui, Y., *Biochim. Biophys. Acta* **2013**, *1827*, 882-891.
- (25) Kütt, A.; Leito, I.; Kaljurand, I.; Soovali, L.; Vlasov, V. M.; Yagupolskii, L. M.; Koppel, I. A., *J. Org. Chem.* **2006**, *71*, 2829-2838.
- (26) Bordwell, F. G.; Hughes, D. L., *J. Org. Chem.* **1982**, *47*, 3224-3232.
- (27) Singh, R.; Whitesides, G. M., *Sulphur-Containing Functional Groups*. John Wiley & Sons: 1993; p 633-658.
- (28) Fernandes, P. A.; Ramos, M. J., *Chem. Eur. J.* **2004**, *10*, 257-266.
- (29) Singh, R.; Whitesides, G. M., *Techniques in Protein Chemistry*. Elsevier: 1995; p 259-266.

- (30) Antonello, S.; Benassi, R.; Gavioli, G.; Taddei, F.; Maran, F., *J. Am. Chem. Soc.* **2002**, *124*, 7529-7538.
- (31) Howie, J. K.; Houts, J. J.; Sawyer, D. T., *J. Am. Chem. Soc.* **1977**, *99*, 6323-6326.
- (32) (a) Antonello, S.; Daasbjerg, K.; Jensen, H.; Taddei, F.; Maran, F., *J. Am. Chem. Soc.* **2003**, *125*, 14905-14916. (b) Christensen, T. B.; Daasbjerg, K.; Valentin-Hansen, P.; Pedersen, E. B.; Rissanen, K.; Shi, W.; Styring, S.; Tommos, C.; Warncke, K.; Wood, R. B., *Acta Chem. Scand.* **1997**, *51*, 307-317.
- (33) Delaive, P. J.; Foreman, T. K.; Giannotti, C.; Whitten, D. G., *J. Am. Chem. Soc.* **1980**, *102*, 5627-5631.
- (34) Pellegrin, Y.; Odobel, F., *C. R. Chimie* **2017**, *20*, 283-295.
- (35) (a) Bausch, M. J.; Guadalupefasano, C.; Gostowski, R., *Energy Fuels* **1991**, *5*, 419-423. (b) dos Santos, R. M. B.; Muralha, V. S. F.; Correia, C. F.; Guedes, R. C.; Cabral, B. J. C.; Simoes, J. A. M., *J. Phys. Chem. A* **2002**, *106*, 9883-9889.
- (36) (a) Nicovich, J. M.; Kreutter, K. D.; Vandijk, C. A.; Wine, P. H., *J. Phys. Chem.* **1992**, *96*, 2518-2528. (b) Berkowitz, J.; Ellison, G. B.; Gutman, D., *J. Phys. Chem.* **1994**, *98*, 2744-2765.